Characterizing Site Suitability for Stormwater Infiltration

A Dissertation
SUBMITTED TO THE FACULTY OF THE
UNIVERSITY OF MINNESOTA
BY

Nicholas Pryor Tecca

IN PARTIAL FULLFILLLMENT OF THE REQUIREMENTS
FOR THE DEGREE OF
DOCTOR OF PHILOSOPHY

Dr. John S. Gulliver and Dr. John L. Nieber

October 2021

Acknowledgements

I would like to express my sincere gratitude to my advisors Professor John Gulliver and Professor John Nieber for their guidance, wisdom, and support. Their efforts to establish the foundations of the research presented in this dissertation long pre-date my involvement, and my time at the St. Anthony Falls Laboratory would not have been possible without their commitment to advancing stormwater research. From advocating for funding, opening opportunities to present and publish, to discussing ideas at Lori's coffee shop, I appreciate all their mentorship.

I am grateful to Professor Xue Feng and Professor Vaughan Voller for volunteering to serve on my committee. Their input and instruction have strengthened my research and challenged me to be a better academic.

I would like to thank Dwayne Stenlund of the Minnesota Department of Transportation and the entire Technical Advisory Panel for keeping this research grounded in the issues facing practicing engineers. I believe research has the biggest impact when it can be implemented, and if this research is pulled off the proverbial shelf it will be due to this focus on application.

This opportunity to study, research, and contribute to stormwater research would not have been possible without funding from the Minnesota Department of Transportation, Local Road Research Board, and the University of Minnesota Department of Civil, Environmental, and Geo-Engineering. Thank you for the generous support.

Collaborative research is not possible without the assistance of excellent collaborators willing to generously contribute their effort and expertise. I am truly grateful to Dr. David Fairbairn of the Minnesota Pollution Control Agency and Nick Tiedeken of the Minnesota Department of Transportation for their assistance accessing sites and gathering data necessary to complete the geostatistical analysis. I appreciate the data and wisdom shared by Chris Lord, Jared Wagner, and Mitch Haustein from the Anoka Conservation District, which was critical to validating the planning phase tool. I would like to thank the Minnesota Supercomputing Institute for technological resources and support that were utilized in the numerical experiments.

Thank you to all the SAFL staff who provide so much support from assistance with equipment, technology, or administration. At various points when I wasn't sure how to move the research forward, Ben Erickson and Patrick Arnold each provided invaluable assistance.

Thank you to the graduate students who studied stormwater infiltration at SAFL before me and provided an amazing foundation to start my research including Brooke Asleson, Rebecca Nestingen, Nicholas Olson, Dr. Farzana Ahmed, and Dr. María García-Serrana.

My success would not have been possible without the support, guidance, and friendship within the SAFL stormwater research group. Thank you to Dr. Andy Erickson and Dr. Poornima Natarajan for your insight and assistance with my many inquiries. Thank you to Vini Taguchi for contemplating brilliant research and life's deep mysteries while cycling across campus. Thank you to Melissa Friese, Nam Nguyen, Nick Bentelspacher, Laura Lewis, Anna Healy, Katie Kemmitt, Samuel Wang, and Peter Olson who contributed their time, energy, and sweat collecting field measurements.

Finally, thank you to all the other graduate students at SAFL that made this an amazing journey. Whether it was advice, studying, potlucks, volleyball, or sharing caffeine in the break room, you all made SAFL an amazing community.

Dedication

To my parents, John and Lynn, for all the support.

To my sisters, Jess and Liz, for always being there.

To my buddy, Lu, for being the best poodle he knows how to be.

To my caring, supportive, and loving wife, Heather, for always dreaming with me.

Abstract

Infiltration stormwater control measures (SCMs) have the potential to provide numerous hydrologic benefits to urban environments by promoting infiltration and evapotranspiration, processes that are not well represented in the water budget of urban areas. Unfortunately, infiltration SCMs presently have a relatively high failure rate which likely has slowed their rate of implementation. This research is focused on addressing several common factors contributing to infiltration SCM failure: identifying a suitable site for an infiltration SCM, quantifying the systemic bias of common methods used to estimate field saturated hydraulic conductivity (K_{fs}), and estimating the spatial correlation of K_{fs} in green infrastructure (GI).

A planning phase tool, referred to as the preliminary infiltration rating (PIR), was developed to assess the likelihood of success of a future surface infiltration SCM at a given location. The PIR was calibrated and validated using rain garden maintenance inspections. The validation set resulted in the PIR predicting an accurate or conservative estimate of the rain garden performance in 85% of rain gardens. Numerical experiments were used to quantify the bias of seven common infiltration measurement methods, removing natural variability and random error from the analysis. In sand through silt loam soils that are typical of infiltration SCMs, the simulated methods have a bias varying from 0.7 to 6.2. Geostatistics were utilized to investigate the spatial correlation of K_{fs} at 9 GI sites. Horizontal, isotropic, variograms of the surface K_{fs} were constructed at each site from modified Philip-Dunne infiltrometer measurements to evaluate the spatial correlation range, the separation distance at which measurements become spatially independent. The spatial correlation range of K_{fs} in GI was estimated to vary from less than 1 meter and up to 22.9 meters, with most sites having a spatial correlation range less than 5 meters.

Identifying potential infiltration areas early in the planning phase allows the selected area to be integrated with other design elements. Characterizing the infiltration potential of a given site requires an understanding of the accuracy of the selected measurement method and an understanding of the in-situ spatial heterogeneity. This research is applicable throughout the land development process on project types including transportation, residential, commercial, industrial, and institutional development in both the public and private sectors.

Table of Contents

List of Tables

List of Figures

Chapter 1 Introduction

Background

Infiltration of stormwater occurs at the air-soil boundary and partitions flow between the surface and subsurface. Infiltration is a key process in the water cycle of most watersheds. As urbanization increases the extent of impervious surface and the compaction of pervious soils, the fraction of stormwater that infiltrates to the subsurface decreases and the fraction to surface runoff increases (Sauer, Thomas, Stricker, & Wilson, 1983). The increased fraction of surface runoff increases the peak flow rate, increases the runoff volume, and increases the associated pollutant loading that reaches receiving waters. These increases can contribute to increased flood risk, altered stream morphology, and eutrophication of receiving waters. Stormwater volume reduction, such as through infiltration, is the only method to reduce both the peak flow rate and runoff volume associated with urbanization (Booth, 1991) and can mitigate some of the stormwater issues associated with urbanization.

Green infrastructure (GI) is an approach to development that attempts to mimic natural processes, such as infiltration and evapotranspiration, to mitigate the impacts of urbanization (U.S. Environmental Protection Agency, 2020). GI attempts to manage stormwater at its source through structural practices, such as infiltration stormwater control measures (SCMs), and non-structural practices, such as minimizing disturbance and minimizing soil compaction. Infiltration SCMs can include a variety of practices including rain gardens, bioinfiltration basins, infiltration basins, and infiltration swales, amongst others (Lindsey, Roberts, & Page, 1992; U.S. Environmental Protection Agency, 2020). An example of a typical, established, vegetated rain garden, is pictured in Figure 1.1. These physical devices attempt to replicate the natural water balance in an urban environment, reducing surface runoff, reducing pollutant loading to receiving water bodies, and increasing infiltration. These infiltration SCMs promote infiltration, evapotranspiration, settling of solids, and capture of dissolved pollutants resulting in reduced flood risk and improved surface water quality. There is broad interest in implementing infiltration SCMs to help mitigate the impacts of urbanization on the stormwater system and downstream receiving waters.

Figure 1.1 Typical, established, vegetated rain garden located in the Como Park Neighborhood, St. Paul, MN

Unfortunately the observed failure rate in infiltration SCMs is in the range of 10% to 50% (Bean & Dukes, 2016; CTC & Associates LLC, 2018; Hilding, 1994; Lindsey et al., 1992). This failure represents a duration of time where the hydrologic goals of the infiltration SCM are not being met, as well as a capital expense to remediate the failure. There are numerous factors that may contribute to this high failure rate including improper siting, low saturated hydraulic conductivity soils in the soil profile, groundwater mounding, sedimentation, and compaction during construction (CTC & Associates LLC, 2018). Improving our understanding of the factors that contribute to success and failure of infiltration SCMs may increase the implementation rate and expand the number of communities that receive the many potential benefits.

Hydraulic conductivity quantifies the movement of water through soil and has units of length per time. The saturated hydraulic conductivity (K_{sat}) defines the minimum rate for water entering the soil mass under a unit hydraulic gradient and the limiting rate for water moving through the soil

mass. Darcy (1856) established that the infiltration rate through a saturated porous media is a function of the K_{sat} and the hydraulic gradient as shown in Equation 1.1 for infiltration applications. Green & Ampt (1911) extended this work to describe saturated flow into an unsaturated porous media using the assumption of a sharp wetting front as shown in Equation 1.2. Richards (1931) described variably saturated flow in a porous media where the hydraulic conductivity is a function of soil moisture as a more realistic approximation of in-situ conditions as shown in Equation 1.3. van Genuchten (1980)parameterized the hydraulic conductivity as a non-linear function dependent on soil matric head as shown in Equation 1.4. Considering these 1-dimensional equations in combination, porous media flow is described as a non-linear, spatially, and temporally variable process.

Equation 1.1

$$q = -K_{sat} i$$

Where q is infiltration rate, and i is the hydraulic gradient defined as the gradient of pressure head over distance.

Equation 1.2

$$q = K_{sat}\left[\frac{-\psi \Delta\theta}{F} + 1\right]$$

Where ψ is the soil matric pressure head (negative soil suction head) at the wetting front, $\Delta\theta$ is the change in volumetric soil moisture as a fraction of total volume, and F is the volume of water previously infiltrated.

Equation 1.3

$$\frac{\delta\theta}{\delta t} = \frac{\delta}{\delta z}\left[K(\theta)\left(\frac{\delta h}{\delta z} + 1\right)\right]$$

Where θ is the volumetric soil moisture, h is the matric pressure head, t is time, z is elevation, and $K(\theta)$ is the hydraulic conductivity as a function of volumetric soil moisture.

Equation 1.4

$$K(S_e) = K_{sat} S_e^l \left[1 - \left(1 - S_e^{1/m}\right)^m\right]^2 = K_{sat}\left(\frac{\theta - \theta_r}{\theta_s - \theta_r}\right)^l \left[1 - \left(1 - \left(\frac{\theta - \theta_r}{\theta_s - \theta_r}\right)^{1/m}\right)^m\right]^2$$

Where S_e is the effective saturation, θ_r is the residual water content defined as the water content for which the gradient $\delta\theta/\delta h$ becomes zero, θ_s is the saturated water content, l is the pore connectivity parameter, m is an empirical shape factor, and $K(S_e)$ is the hydraulic conductivity as a function of effective saturation.

The field saturated hydraulic conductivity (K_{fs}) is the in-situ K_{sat} that accounts for the soil structure. The K_{fs} is a highly heterogeneous soil property with observed variability of up to two orders of magnitude over horizontal separation distances less than 3 meters (Asleson et al., 2009; Gupta et al., 2006; Press, 2019). Within a soil texture class, the interquartile range of K_{fs} can vary by a factor of 2.0 to 25.3 (Rawls, Gimenez, & Grossman, 1998). Intra-annual variability in infiltration rate has been observed on the order of a factor of 2, with variations following changes in temperature induced viscosity (Emerson & Traver, 2008). K_{fs} can be increased due to vegetative life cycles or bioturbation (Sobieraj, Elsenbeer, Coelho, & Newton, 2002), and decreased due to deposition or compaction (Gupta et al., 2006; Pitt, Chen, Clark, Swenson, & Ong, 2008). The natural heterogeneity, seasonal fluctuations, and temporal variations contribute to the difficulty, expense, and time required to measure K_{fs}.

While there are many factors that contribute to infiltration SCM success relating to soils (K_{fs}, layering, groundwater interactions), land use (percent impervious, pollutant loading), design decisions (loading ratio, pre-treatment), construction considerations (sequencing, minimizing compaction), accurately characterizing K_{fs} may be the most influential. However, there are numerous practical difficulties in estimating K_{fs}. Several common methods to estimate K_{fs} utilize a steady-state flow assumption and have a 6-hour minimum duration (ASTM International, 2018b; USBR 7300-89, 1989). Infiltration SCMs are often designed with the native soil interface below existing surface grade, requiring either excavation, boring, augering, or another method of accessing soils lower in the profile. The timeline from the beginning of design to construction of an infiltration SCM can span multiple years. Possibly due to the practical difficulties, some jurisdictions allow a single point measurement to characterize K_{fs} (Minnesota Pollution Control Agency, 2018), or soil texture (Minnesota Pollution Control Agency, 2017; Wisconsin Department of Natural Resources, 2017) or soil grain size analysis (Washington State Department of Ecology, 2019) to be used as a proxy for K_{fs}. However, a large point measurement sample size is required to reduce the uncertainty in K_{fs} to an acceptable level (Ahmed, Gulliver, & Nieber, 2015). The time-consuming methods and large recommended sample size contribute to the cost of exploratory infiltration measurements approaching or exceeding the cost of structural measures to

reduce the risk of excessive ponding, such as providing a backup underdrain. However, an active underdrain would create a detention SCM, not an infiltration SCM, which does not provide the stormwater volume reduction benefits that maximize the potential hydrologic benefits. Therefore, low-cost methods are needed to characterize the potential of a site for supporting an infiltration SCM.

This research is intended to provide guidance directly applicable to the implementation of infiltration SCMs with the goal of reducing the overall failure rate. Infiltration SCMs are often sited prior to field investigation, then the field investigation is used to verify infiltration capacity. Improved guidance on methodology to identify infiltration SCM sites prior to field investigation can allow the site to be integrated with other design elements and yield more sites that are confirmed to be suitable by field investigation. There are various infiltrometers and permeameters to estimate the K_{fs}, but the associated accuracy is not well documented by ASTM International or other applicable standards. An understanding of the systemic bias associated with each infiltrometer and permeameter can inform selection and contribute to quantifying the uncertainty associated with field measurements. Substantial variability in minimum spacing or sample size required to characterize K_{fs} exists between jurisdictions, and much of the existing guidance has a large associated uncertainty. An understanding of the spatial correlation of K_{fs} typical of urban systems can provide quantitative guidance on sample spacing. The research presented herein is intended to reduce the uncertainty associated with the design of infiltration SCMs to promote their implementation.

Overview

The research presented herein is based in part on a research project funded by the Minnesota Department of Transportation (MnDOT) and the Local Road Research Board (LRRB) titled "Design and Construction of Infiltration Facilities". The Principal Investigators on the project were John S. Gulliver and John L. Nieber.

Chapter 2 describes a planning phase tool that can be used to identify areas that are likely suitable for a surface infiltration SCM. The tool aggregates two soils datasets and two variables derived from an elevation dataset to estimate the Preliminary Infiltration Rating (PIR), which is a categorical rating of a potential site to be suitable for an infiltration SCM. The tool was developed to be implemented in a geographic information system (GIS) such that other applicable spatial datasets, such as environmentally sensitive areas or property information, could be overlaid on

the output. The weights associated with the input variables and output categories were calibrated and validated using a rain garden maintenance dataset provided by the Anoka Conservation District. The PIR assigned a correct or conservative categorical classification for 85% of the rain gardens in the validation dataset.

A version of Chapter 2 has been published in 2021 in the Journal of Sustainable Water in the Built Environment, 7(2), under the title "Siting surface infiltration-based stormwater control measures using a geographic information systems approach". The author of this dissertation was the lead author for this publication and was involved throughout the research. Assistance was provided by co-authors in developing the concept of the research, evaluating the results, as well as editing the text of the publication.

Chapter 3 describes the evaluation of systemic bias in commonly used methods to measured K_{sat} using numerical experiments. The source of the systemic bias is believed to be due to the assumptions made by each method and has not been quantified by previous research. Understanding the systemic bias will allow practitioners to quantify the uncertainty associated with each method. This can be used as a guide in selecting the preferred infiltration measurement method, or as a guide in selecting an appropriate factor of safety on the measured K_{sat}.

A version of Chapter 3 is in preparation for submission to Vadose Zone Journal under the title "Bias of Stormwater Infiltration Measurement Methods Evaluated using Numerical Experiments". The author of this dissertation was the lead author for this publication and was involved throughout the research. Support was provided by the co-authors throughout including establishing the numerical experiment, interpreting the results, and preparing the text of the manuscript. Technologic support and resources provided by the staff of Minnesota Supercomputing Institute (MSI) was important to the success of this manuscript.

Chapter 4 evaluates the spatial correlation structure of K_{fs} in urban systems typical of post-construction green infrastructure. A modified Philip-Dunne infiltrometer was utilized to measure the K_{fs} at rain gardens, turf grass park areas, and grass swales. Variograms were constructed for each site to evaluate the variance as a function of separation distance. The variograms were used to estimate the spatial correlation range, which is the separation distance at which measurements become spatially independent. The spatial correlation range can be used to establish sampling plans to characterize K_{fs}.

A version of Chapter 4 is in preparation for submission to Soil Science Society of America Journal under the title “Spatial Correlation of Field Saturated Hydraulic Conductivity in Disturbed Urban Soils”. The author of this dissertation was the lead author for this publication and was involved throughout the research. Co-authors provided input on the concept, interpreting the results, and preparing the manuscript text. Assistance in collecting K_{fs} field measurements using the modified Philip-Dunne (MPD) infiltrometer was provided by Melissa Friese, Nam Nguyen, Nick Bentelspacher, Laura Lewis, Anna Healy, Katie Kemmitt, Samuel Wang, and Peter Olson. Data was reanalyzed from previous publications by Brooke Asleson and Nicholas Olson, and their thorough work is greatly appreciated.

Chapter 5 provides summary and overall conclusions from the research discussed in this dissertation.

Chapter 2 Planning Phase Siting of Infiltration SCMs

Summary

Infiltration stormwater control measures (SCMs) are commonly the preferred practice implemented to mitigate the hydrologic impacts of urbanization, such as increased surface runoff volumes from small to moderate rain events and degraded surface water quality. Infiltration SCMs, however, can fail for a number of reasons including improper siting or inadequate maintenance resulting in large capital expense and also a time period where the hydrologic and water quality benefits are not being realized. Identifying a suitable site is one critical factor in the long-term success of an infiltration SCM. This chapter develops a preliminary infiltration rating, or PIR, which is a composite rating calculated in a geographic information system that assesses the likelihood of success of a future surface infiltration SCM at a given location. The input variables to the PIR include the surface saturated hydraulic conductivity (K_{sat}), depth to water table, topographic slope, and relative elevation, all of which are readily available from online sources. The PIR was calibrated and validated using maintenance inspections from 104 rain gardens completed by the Anoka Conservation District in Minnesota. The validation set resulted in the PIR predicting an accurate or conservative estimate of the rain garden performance in 85% of rain gardens. The PIR can serve as an effective planning tool for siting future surface infiltration SCMs in the land development process and can guide the site-specific investigation.

Introduction

Infiltration stormwater control measures (SCMs) mitigate some of the impacts of urbanization, increasing the fraction of rainfall that infiltrates to the subsurface relative to urban areas without infiltration SCMs (Booth, 1991). Many communities require a runoff volume reduction practice, such as an infiltration SCM, to be the preferred practice included when a development exceeds a threshold of new impervious area. In addition to the volume reduction benefits, infiltration SCMs contribute to the removal of particulate and dissolved pollutants from stormwater surface runoff.

Infiltration SCMs include a variety of different structural practices such as infiltration basins, infiltration trenches, bio-infiltration basins, rain gardens, bio-infiltration swales, and subsurface infiltration systems. The present chapter will focus on surface infiltration systems and has limited applicability to subsurface infiltration systems. Studies have shown the infiltration SCM failure

rate to be in the range of 10 to 50 percent (Bean & Dukes, 2016; CTC & Associates LLC, 2018; Hilding, 1994; Lindsey et al., 1992). This failure rate results in both capital costs to remedy the failure, and a time period where the water quantity and quality goals are not being met. There are a variety of failure modes for infiltration SCMs, and multiple failure modes can simultaneously contribute to failure. Issues contributing to failure may include soils with a layer having a low saturated hydraulic conductivity (K_{sat}) in the soil profile, groundwater mounding, sedimentation, and compaction during construction (CTC & Associates LLC, 2018). Selecting an appropriate site can alleviate many of these issues, notably issues related to the soil profile and groundwater interactions. Identifying an appropriate site by manually reviewing available data in a simple desktop analysis can be a time-consuming and tedious process particularly for large areas. Automating the process by identifying the critical datasets and compiling the data into a composite rating can save time and produce consistent results.

Research providing example assessment systems that use spatial data to identify areas with the potential to support managed aquifer recharge (MAR) was identified in the literature. Ghayoumian et al., (2007) proposed a fuzzy logic product operator such that a non-favorable variable would have a rating significantly less than 1 and therefore a large influence on the overall rating. It was proposed that the MAR potential should be evaluated based on the soil infiltration rate, topographic slope, dry alluvial thickness, and electrical conductivity. Electrical conductivity was used to quantify groundwater salinity, which is most applicable in coastal regions where water recovery for reuse is intended. Direct surface recharge basins were the method selected to achieve the MAR goals, and these operate very similar to many infiltration SCMs.

Miller (2014) completed a GIS based analysis for use in soil mapping that calculated relative elevation and validated the procedure with the field assessment of soil scientists. The relative elevation describes the position of a point on the hillslope where larger positive values indicate areas closer to the top of a local hill and larger magnitude negative values indicate areas closer to a local depression. The proposed relative elevation was calculated as a function of the elevation at a point and the maximum and minimum elevations within a neighborhood of 135 meters of the point of interest. The 135 meter neighborhood was identified by Miller (2014) as the optimal analysis scale for relative elevation by validating the GIS calculation with field observations by a soil scientist.

This chapter proposes a fuzzy logic model implemented in a geographic information system (GIS), the output of which is a raster that can be displayed on a map. Select elements from the MAR study proposed by Ghayoumian et al., (2007) are utilized. The relative elevation proposed by Miller (2014) is incorporated into the proposed fuzzy logic model to account for the ability to direct stormwater to an area by gravity drainage. Environmentally sensitive layers applicable to the region of interest can be superimposed on the model, identifying locations where caution in siting infiltration practices is prudent.

The purpose of this analysis is to provide engineering designers and planners with a rapid screening tool that can be used before or early in the design process to identify sites where infiltration SCMs are likely to be successful. This tool can also be used to guide the site-specific field investigation. This may also serve as a communication tool between engineers, developers, landowners, and regulators including those with non-technical backgrounds. Identifying appropriate sites early in the design process allows infiltration SCMs to be proactively incorporated into the development plan.

Methods

Geographic Information System Analysis

The geographic information system (GIS) analysis is implemented using ESRI ArcMap v10.5.1 (ArcMap). The ArcMap software was selected as it is commonly used by industry professionals and allows a user to overlay additional information, if necessary. The ModelBuilder application within ArcMap was used to implement the workflow.

Spatial Data

Four variables were identified as important to the success of surface infiltration SCMs. These four variables were adapted from Ghayoumian et al., (2007) and Miller (2014), aggregated following guidance from Ghayoumian et al., (2007), and validated with a rain garden maintenance dataset from the Anoka Conservation District (2019). The K_{sat} of the soil within 2-meters of the surface is used to describe the limiting rate that stormwater can infiltrate into the subsurface. The depth to groundwater describes the likelihood of groundwater-surface water interactions occurring as a result of the infiltration SCM. The topographic slope relates to the constructability and safety of an infiltration SCM, as moderately steep slopes require larger

footprints than minimal slopes to construct flat infiltration SCMs and infiltrating additional water near steep slopes may contribute to slope stability issues. The relative elevation describes the position on the hillslope and the potential to direct surface runoff to an area under gravity flow conditions. A flow chart describing how these variables are aggregated is provided in Figure 2.1.

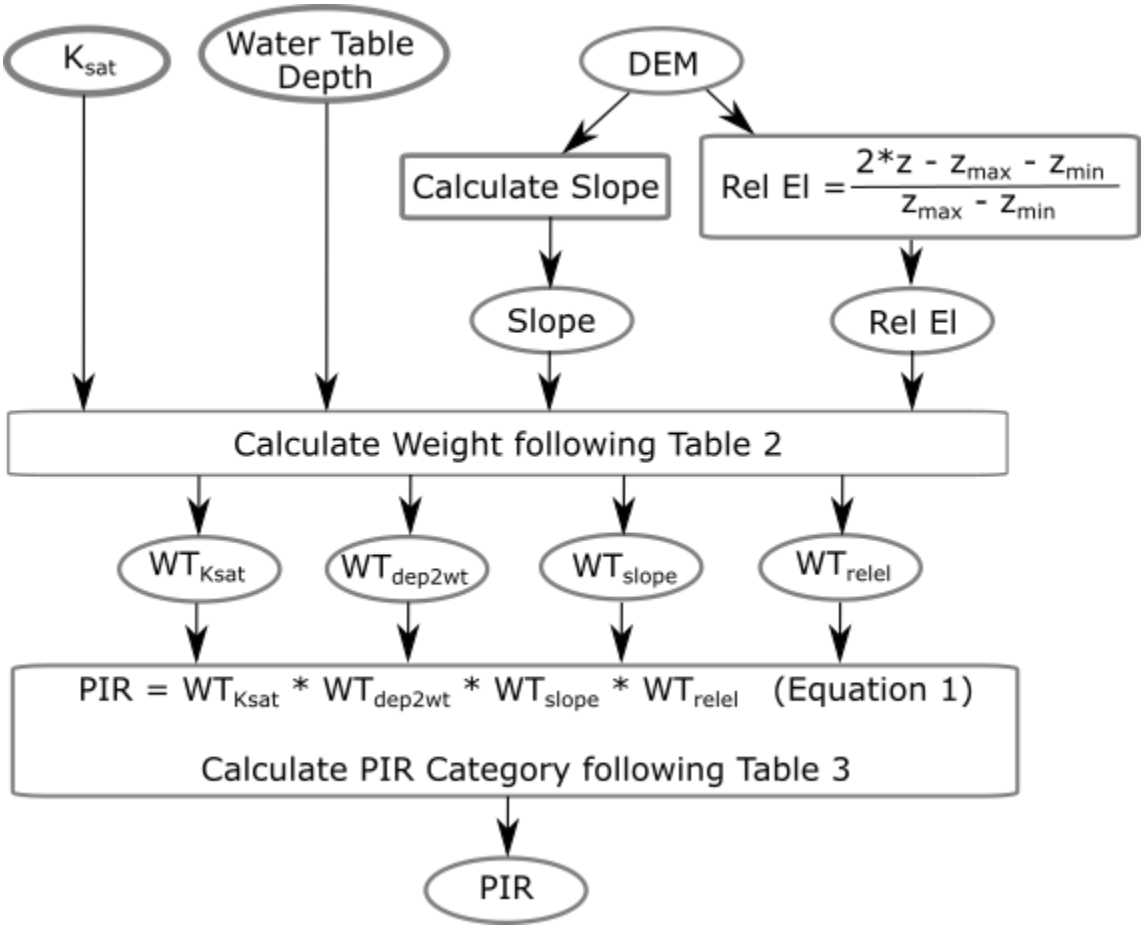

Figure 2.1 Overview of the key components required to calculate the preliminary infiltration rating (PIR). Ovals represent data and rectangles represent calculations.

Many jurisdictions prohibit infiltration SCMs in environmentally sensitive areas. Spatial data identifying these environmentally sensitive areas may overlay the output composite rating to identify areas where infiltration SCMs are likely to be prohibited. Environmentally sensitive layers will vary based on region and jurisdiction but may include information identifying wetlands, shallow bedrock, karst regions, contaminated soils, and source water protection areas.

Data from Anoka County, Minnesota was used to calibrate and validate the proposed fuzzy logic model, but the workflow should be applicable in other regions where the required spatial data is

available. Anoka County is part of the Minneapolis-Saint Paul metropolitan area, located in the Upper Midwest of the conterminous United States. The workflow that was developed can be implemented over a range of scales from the resolution of the output raster to county-wide scale. Example applications described herein include a transportation redevelopment and municipal site development. Larger scales are possible although they have not been evaluated in this chapter.

Soils Data

Soils data obtained from the Natural Resources Conservation Service (NRCS) Soil Survey Geographic Database (SSURGO) dataset was acquired for this workflow (U.S. Department of Agriculture, 2019). SSURGO data is available for approximately 92% of counties in the United States of America and territories as of November 2019. The SSURGO dataset was created within the NRCS using field and remote-sensing techniques to identify areas with similar soil types, and typically describes soil layering within 2-meters of the surface. The Soil Data Viewer tool in ArcMap is used to extract the K_{sat} and depth to water table. Both variables are aggregated for the dominant component of the soil map unit. K_{sat} is aggregated as a weighted average over all soil layers. The weighted average was selected as it is available within the Soil Data Viewer tool, although the analysis may be improved by using the geometric mean, if available. The depth to water table is conservatively selected as the lowest value (e.g., highest elevation) over the calendar year. The vector layer is converted to a raster with a 10-meter resolution, which approximates the level of detail provided in the vector polygons.

Terrain Data

The workflow utilizes a digital elevation model (DEM) with a 3-meter horizontal resolution to capture the local variability of terrain features. Alternative resolutions likely could be utilized but have not been evaluated as part of the present study. In this study a LiDAR derived DEM was retrieved from MnTOPO (Minnesota Department of Natural Resources, n.d.). DEM data is often available from state or local governments. The slope is calculated using the ArcMap D8 slope routine. The relative elevation proposed by Miller (2014) was calculated from the DEM and normalized by the difference between the minimum and maximum elevations in the 135 meter local neighborhood. The 135 meter local neighborhood was identified by Miller (2014) as the optimal scale to analyze relative elevation by comparing field observations to GIS calculated values. Normalizing the relative elevation converts the relative elevation to a dimensionless

number in the range of -1 (lowest elevation) to 1 (highest elevation), representing the position on the hillslope. Both the slope and relative elevation are resampled using a bilinear interpolation to a 10-meter resolution and snapped to the soils raster.

Fuzzy Logic Model

The proposed model was developed to represent the potential for a location on the landscape to support a surface infiltration SCM. The model automates the process of a manual desktop analysis, producing consistent results, and providing a visual method for reviewing alternative surface infiltration SCM sites. In contrast to classical logic where a parameter is classified as either false or true, fuzzy logic allows for a parameter to be considered partially true. When stated mathematically, classical logic only allows the values of 0 or 1, whereas fuzzy logic can use any value on the range of 0 to 1 (Ross, 2017). Infiltration SCMs have a range of potential performance with a gradual transition from excellent to poor. The parameters contributing to the overall performance exhibit a similar gradual transition from excellent to poor. A fuzzy logic model was thus selected to aggregate the variables into a composite rating. A product operator was chosen to combine the fuzzy logic variables, as this allows a single unacceptable value to rate a given location as a poor site for an infiltration SCM. The composite rating, named the Preliminary Infiltration Rate or PIR, is defined in Equation 2.1.

Equation 2.1

$$PIR = WT_{Ksat} * WT_{dep2wt} * WT_{slope} * WT_{relel}$$

The variables WT_{Ksat}, WT_{dep2wt}, WT_{slope}, and WT_{relel} are weights associated with the K_{sat}, depth to water table, topographic slope, and relative elevation, respectively. The PIR defined in Equation 2.1 outputs a number that is compiled into a category. Four categories are utilized to represent the relative likelihood of successfully implementing an infiltration SCM. The categories were established such that if a single input variable has a poor quality represented by a weight of 0.01, the composite category would be designated as Poor. However, if all input variable weights are greater than 0.01, the area will be rated as Moderate, Good, or Excellent.

Calibration of Infiltration SCM Data

A set of maintenance inspection reports for existing infiltrating rain gardens (Anoka Conservation District, 2019) was obtained to calibrate and validate the fuzzy logic model defined in Equation

2.1. Anoka County is located in the Minneapolis-Saint Paul metropolitan area of Minnesota. The Anoka Conservation District has compiled a dataset (Anoka Rain Gardens) of 115 existing infiltrating rain gardens for maintenance purposes. Rain gardens are the only type of surface infiltration SCM that was included in the Anoka Rain Gardens dataset, and rain garden performance was assumed to be representative of other types of surface infiltration SCMs. Among these there were 9 rain gardens that did not have SSURGO data available and 2 rain gardens that had not been inspected since construction, resulting in 104 rain gardens with sufficient data for this analysis. The rain gardens were constructed between 2010 and 2018. Visual inspections occurred between 2016 and 2019. Visual inspections resulted in rain gardens being assigned a letter grade that represents the performance and maintenance needs of the rain garden. The five letter grades used by the Anoka Conservation District correspond with the four PIR categories as shown in

Table 2.1. The most recent inspection letter grade was used for rain gardens that had multiple inspections. In 5 cases, the most recent inspection notes indicated a lower letter grade was given due to pretreatment maintenance issues rather than a lack of infiltration capacity. In these 5 cases the next most recent inspection rating was utilized. In an additional 4 cases, an underdrain was installed after initial construction. It was presumed the retrofitted underdrain indicated the rain garden had not been functioning adequately and these rain gardens were rated as Poor. The Anoka Rain Gardens were randomly separated into a calibration set containing two thirds of the data and a validation set containing one third of the data as shown in Figure 2.2. The number of rain gardens associated with each Anoka Letter Grade and PIR category are shown in

Table 2.1.

Table 2.1 Anoka Conservation District rain garden maintenance inspection grades, criteria, and associated PIR category

Anoka Letter Grade	Anoka Grading Criteria	PIR Category	Count in Calibration	Count in Validation
A	Excellent. All functions are working. No maintenance is required.	Excellent	18	15
B	Good. The primary functions are working. Some regular maintenance is required.	Good	39	12
C	Fair. Erosion impacts are likely or have already happened and/or other functions are not working; light maintenance is required.	Moderate	4	6
D	Poor. Erosion impacts are likely or have already happened and/or other functions are not working; structural maintenance, retrofit, or re-design is necessary.	Poor	3	0
F	Failing. The rain garden is not providing any functions and/or the rain garden is not present.	Poor	6	1

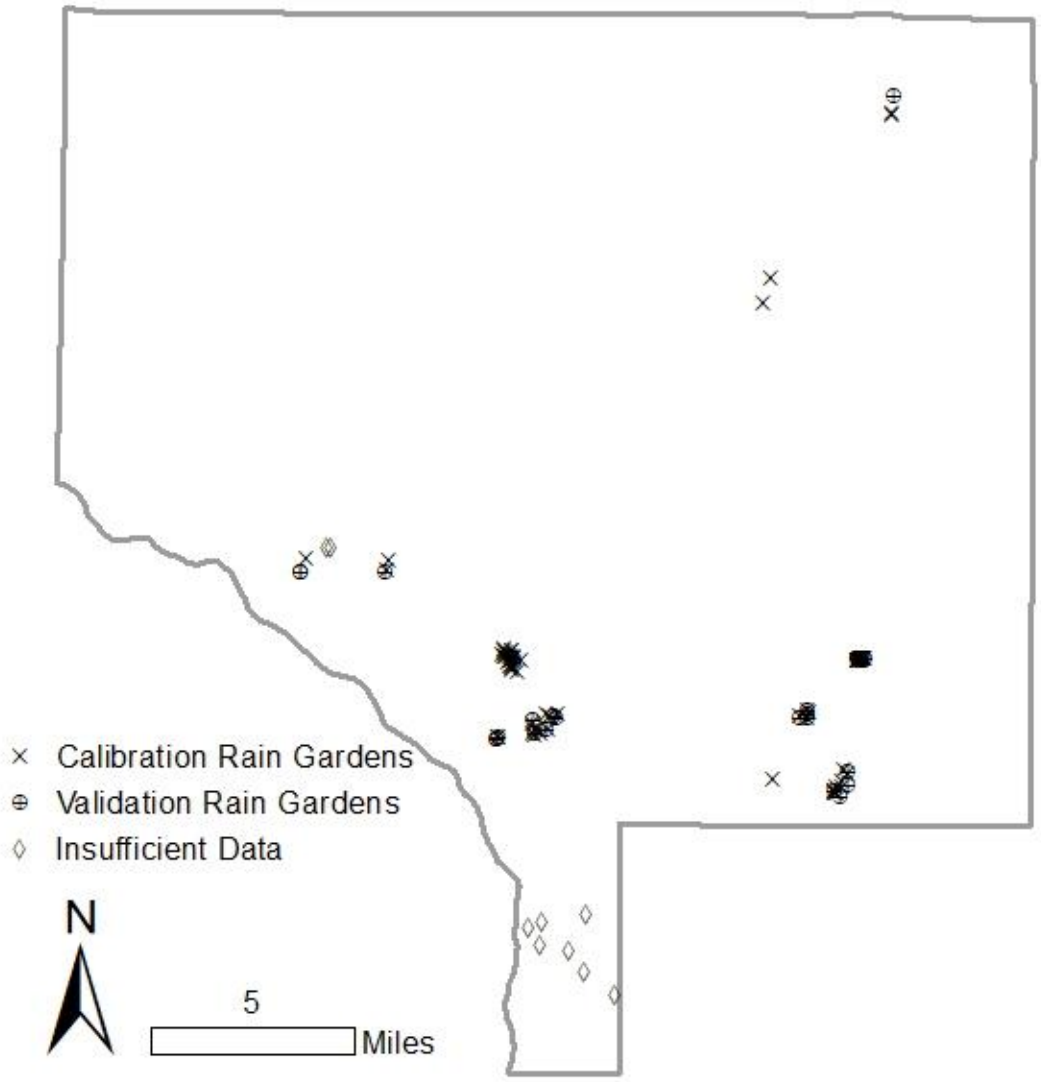

Figure 2.2 Rain gardens monitored by the Anoka Conservation District. Figure includes data from: (Anoka Conservation District, 2019; Minnesota Department of Transportation, 2018).

Results and Discussion

The calibration set of 70 rain gardens was used to modify the weights and categories associated with the PIR fuzzy logic model. The goal of the calibration was to provide a rating where the constructed surface infiltration SCM was likely to perform as well or better than predicted by the PIR. Table 2.2 shows the calibrated input variable categories and associated calibrated weight. The calibrated PIR categories are shown in Table 2.3. The calibrated PIR for Anoka County is

shown in Figure 2.3. An error matrix is a common tool for assessing the accuracy of a classification model (Congalton, Oderwald, & Mead, 1983). An error matrix of the calibration dataset is shown in Table 2.4, where the columns of the error matrix represent the true category, in this case the Anoka Rain Gardens inspection category. The rows of the error matrix represent the model predicted category, in this case the PIR predicted category. The values in the error matrix are a count of the number of rain gardens with the given characteristics. The major diagonal from the upper left to lower right therefore represents the instances where the model predicted category matches the true category. The accuracy of the model is defined by the sum of the values along the major diagonal divided by the total number of data points. Cells that are below the major diagonal represent rain gardens where the model conservatively predicted a level of performance less than what was observed. Cells that are above the major diagonal represent rain gardens where the model non-conservatively predicted a level of performance better than what was observed.

Table 2.2 PIR input variable weights. Note: dep2wt = depth to water table; and Rel El = relative elevation

Variable	Weight
$K_{sat} \leq 5$ mm/hr ($K_{sat} \leq 0.2$ in/hr)	0.01
5 mm/hr < $K_{sat} \leq 15$ mm/hr (0.2 in/hr < $K_{sat} \leq 0.6$ in/hr)	0.35
15 mm/hr < $K_{sat} \leq 25$ mm/hr (0.6 in/hr < $K_{sat} \leq 1$ in/hr)	0.45
25 mm/hr < $K_{sat} \leq 45$ mm/hr (1 in/hr < $K_{sat} \leq 1.8$ in/hr)	0.75
45 mm/hr < K_{sat} (1.8 in/hr < K_{sat})	0.95
dep2wt < 100 cm (*dep2wt* < 39.4 in)	0.01
100 cm ≤ *dep2wt* < 200 cm (39.4 in ≤ *dep2wt* < 78.7 in)	0.3
200 cm ≤ *dep2wt* (78.7 in ≤ dep2wt)	0.5
10% < *slope*	0.01
4% < *slope* ≤ 10%	0.3
2% < *slope* ≤ 4%	0.5
Slope ≤ 2%	0.7
0.75 < *Rel El*	0.01
0 < *Rel El* ≤ 0.75	0.3
-0.5 < *Rel El* ≤ 0	0.5
-1 < *Rel El* ≤ -0.5	0.7

Table 2.3 PIR composite rating categories

PIR Category	PIR Value
Poor	PIR ≤ 0.009
Moderate	0.009 < PIR ≤ 0.05
Good	0.05 < PIR ≤ 0.1
Excellent	0.1 < PIR

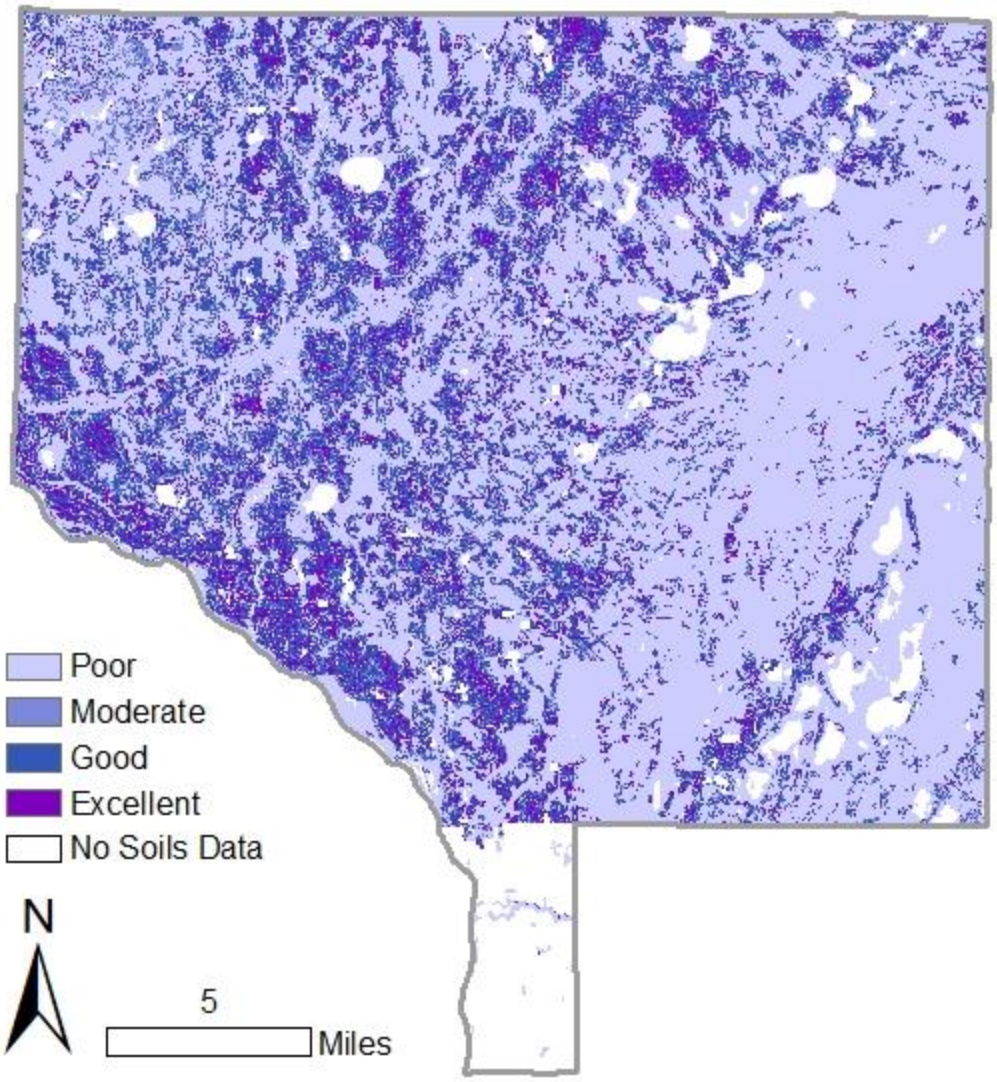

Figure 2.3 Preliminary infiltration rating for Anoka County, Minnesota. Figure includes data from: (Minnesota Department of Transportation, 2018).

Table 2.4 Error matrix of calibration rain gardens. Accurate or conservative results are shown in bold.

	Anoka Inspection Category			
PIR Category	Excellent	Good	Moderate	Poor
Excellent	**1**	5	0	2
Good	**12**	**16**	3	3
Moderate	**4**	**9**	**0**	0
Poor	**1**	**9**	**1**	**4**

The PIR accurately predicted the Anoka Rain Garden category in 30% of instances in the calibration rain gardens. The PIR provided a conservative prediction for 51% of the rain gardens, and a non-conservative prediction for 19% of the rain gardens. The PIR therefore resulted in a correct or conservative category prediction for 81% of the calibration rain gardens, indicated by the bold counts in Table 2.4.

When the PIR incorrectly assigned a Poor category to a rain garden rated as Excellent, Good, or Moderate by the inspections, the depth to water table variable was the most common variable that resulted in a PIR rating of Poor. When the PIR incorrectly assigned a category of Excellent or Good to a rain garden rated as Poor by the inspections, the inspection notes typically mentioned difficulty establishing and maintaining vegetative cover or post-construction structural changes, such as an added underdrain or reduced ponding depth which are indicative of poor infiltration.

A validation set of 34 rain gardens was used to verify the performance of the fuzzy logic model. The error matrix of the PIR for the validation Anoka Rain Gardens is shown in Table 2.5. The validation dataset has an accuracy of 21%. The PIR produced a conservative prediction for 65% of the rain gardens, and a non-conservative prediction for 15% of the rain gardens. A correct or conservative prediction is desirable, where the rain garden performs at least as well as predicted by the PIR. The PIR produced a correct or conservative prediction 85% percent of the time as indicated by the bold counts in Table 2.5, which is close to the calibration value of 81%.

Table 2.5 Error matrix of validation rain gardens. Accurate or conservative results are shown in bold.

	Anoka Inspection Category			
PIR Category	Excellent	Good	Moderate	Poor
Excellent	**3**	2	0	0
Good	**6**	**3**	2	1
Moderate	**2**	**2**	**1**	0
Poor	**4**	**5**	**3**	**0**

Limitations

The Anoka Conservation District maintenance inspection grade is based on a qualitative visual inspection of each rain garden. The criteria for the qualitative visual inspection is provided in Table 2.1, and comments were provided by the inspector to support the rating. Visual inspections are capable of determining the level of infiltration performance by observing factors such as standing water, hydrophytic vegetation, vegetative health, sedimentation, and surface crusting. The qualitative inspection ratings should be considered a general statement of the apparent rain garden performance on the day of the inspection.

Three of the four variables input to the PIR, the depth to water table, relative elevation, and topographic slope, were calibrated using the Anoka Rain Garden dataset. The K_{sat} variable was not calibrated because all 104 rain gardens were located in areas where the K_{sat} in the SSURGO dataset exceeded 45 mm/hr. The K_{sat} weights shown in Table 2.2 were adapted from Ghayoumian et al., (2007) with minor modifications. An additional category was added to include soils with moderate infiltration potential in the range of 5 mm/hr to 15 mm/hr, and the weights were adjusted to account for the additional category.

The output raster is at 10-meter resolution. Infiltration SCMs can vary from less than 10 square meters to 100s of square meters. The raster is not meant to be a definitive statement on the infiltration capability of an exact point. Rather it should be considered a general statement of the capability of an area to support future infiltration SCMs. The fuzzy logic model was established such that the underlying datasets contributing to the rating of a location could be evaluated and the rating confirmed. Therefore, similar results likely could be obtained by critically evaluating

each of the input variables manually. The proposed fuzzy logic model allows large areas to be evaluated rapidly and consistently.

The infiltration rate is a continuous variable, therefore infiltration SCMs have a range of potential functionality. Fuzzy logic allows the PIR to mimic this range of potential functionality and display a range of potential performance. If a classical logic approach is preferable to fuzzy logic, the PIR category of Poor could be considered non-functional, and the PIR categories Moderate, Good, and Excellent could be considered functional.

The PIR is most suitable in urbanizing areas where SSURGO data is available, and when the existing and proposed topography are relatively similar. Ultra-urban areas with disturbed soils are not well represented by the SSURGO dataset. Extensive earthwork during the proposed construction would limit the relevancy of all input variables. The PIR is intended as a preliminary screening tool and is not a replacement for thorough field investigation and proper design. Engineered media selection, pre-treatment performance, and maintenance protocols are not described in this preliminary screening tool but influence the ultimate infiltration performance. These factors should be considered in the design process and life cycle of the infiltration SCM.

Finally, the PIR is based on datasets for which each have an associated uncertainty. Notably the K_{sat} and depth to water table are both highly variable in space and time. An understanding of the uncertainty associated with the inputs is critical to an appropriate understanding of the PIR uncertainty and should be considered in any decision-making process.

Application to Land Development

Land development that increases impervious surface area is often required to mitigate the associated hydrologic impacts using an infiltration SCM. Land development includes transportation, residential, and commercial construction projects in both the private and public sectors, as well as other land altering projects. A planning phase tool such as the PIR that identifies the likelihood of a given site being suitable for an infiltration SCM can guide early land-development planning, enhance communication between technical and non-technical stakeholders, and reduce the number of sites that require detailed field investigation.

Examples implementing the PIR and incorporating overlays for environmentally sensitive areas for a transportation corridor and a municipality are shown in Figure 2.4. Both examples are located within the Minneapolis-Saint Paul metropolitan area as shown in Figure 2.4a. Information

relating to the presence of wetlands, shallow bedrock, karst features, and drinking water supply management areas are all included in the environmentally sensitive areas layer overlaid on the PIR. Figure 2.4b shows a corridor of I-35E that may increase impervious surface requiring consideration of infiltration SCMs. The figure shows that the northern portion of the corridor includes environmentally sensitive areas where infiltration is likely not appropriate. The southern portion of the corridor includes sites with a range of potential infiltration performance. These sites can be evaluated in the context of other project considerations, allowing locations with a high potential for success to be identified early in the planning process. Figure 2.4c shows the City of Woodbury located in Washington County, Minnesota. The figure identifies eastern portions of the city as environmentally sensitive areas, north western portions of the city as having a lower potential to support surface infiltration SCMs, and south-central portions as having higher potential to support surface infiltration SCMs. In both transportation and municipal contexts, the PIR in combination with environmental data provides a rapid screening of areas where infiltration is likely to be successful. A map such as shown in Figure 2.4 can be completed in approximately 2 to 4 hours.

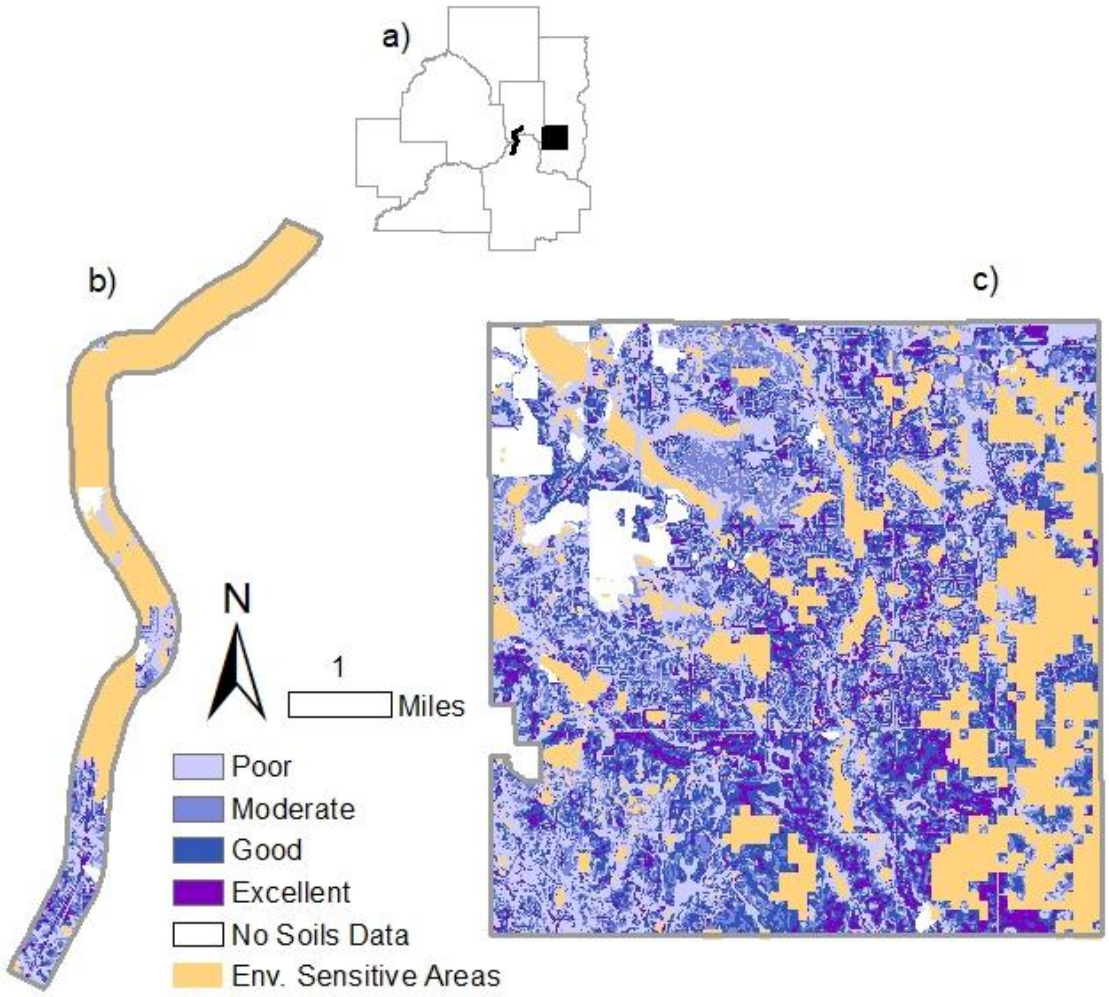

Figure 2.4 Examples implementing the preliminary infiltration rating with overlays of environmentally sensitive areas: (a) Minneapolis–St Paul seven-county metropolitan area with locations of examples; (b) I-35E from 10th Street in St. Paul, Minnesota, to Lone Oak Road in Eagan, Minnesota; and (c) the City of Woodbury, Minnesota. Figure includes data from: (Minnesota Department of Health - Environmental Health Division - Source Water Protection Unit, 2014; Minnesota Department of Health, 2017; Minnesota Department of Natural Resources, 2016, 2017; Minnesota Department of Transportation, 2018; Minnesota Geologic Survey, 2016).

Conclusions

The PIR provides an effective method of identifying areas where surface infiltration SCMs are likely to be successful, prior to any additional site-specific field investigations. The PIR is most

applicable to land development projects, including transportation and site development, that are located in urbanizing areas where the proposed change in topography is relatively minimal such that the SSURGO dataset and DEM provide a reasonable representation of the proposed condition. The map of the PIR categories can be combined with other relevant spatial data, such as environmentally sensitive areas or property information, to identify the most suitable sites for surface infiltration SCMs. The PIR improves on simplistic desktop analyses, such as relying exclusively on hydrologic soil group, by incorporating additional relevant variables into a composite rating that is easy to interpret and requires nominal additional time. The PIR can serve as a communication tool between technical and non-technical stakeholders, as well as a guide to identifying locations for detailed site-specific investigation.

Chapter 3 Evaluating the Bias of Stormwater Infiltration Measurement Methods

Summary

Infiltration stormwater control measures (SCMs) have the potential to contribute towards mitigating the impacts of urbanization on downstream receiving waters. Infiltration SCMs are most often successful when the in-situ saturated hydraulic conductivity (K_{sat}) is well characterized. In this chapter numerical solutions of the Richards equation are used to quantify the bias of seven infiltration measurement methods, removing natural variability and random error from the analysis. The methods evaluated in this study include the double ring infiltrometer, Saturo infiltrometer, modified Philip-Dunne infiltrometer, Turf-Tec IN2-W infiltrometer, USBR 7300-89 well permeameter, Philip-Dunne permeameter, and the Guelph permeameter. These methods encompass surface and borehole configurations. Seven homogenous, isotropic soil textures were simulated at four initial soil moistures for the seven methods, resulting in a full factorial design. The bias is defined as the "measured" K_{sat} determined by a given method divided by the K_{sat} input to the numerical experiments. The "measured" K_{sat} is in quotations to identify the measurement occurs in a numeric experiment rather than in a physical experiment. The "measured" K_{sat} is the output for all methods, as it is assumed the quasi-steady state infiltration rate approaches the K_{sat} as the hydraulic gradient approaches unity. In sand through silt loam soils that are typical of infiltration SCMs, the simulated methods have a bias in the range of 0.7 to 6.2. The Turf-Tec was the only infiltrometer that produced a bias greater than 2.5 for these soils and a correction factor of 3 to 6 may be appropriate for measurements in sand to silt loam. Initial relative soil moisture had a minimal contribution to bias for most methods. Methods that rely on a 1-dimensional flow assumption consistently overestimated the infiltration rate. Borehole methods produced results with bias similar to surface methods. Long duration methods did not consistently produce more accurate results than short duration methods. In silty clay soil, the Saturo infiltrometer, modified Philip-Dunne infiltrometer, Philip-Dunne permeameter, and Guelph permeameter had the least bias; however, the Saturo required substantially less time than these other methods.

Introduction

Infiltrating stormwater control measures (SCMs) have the potential to improve stormwater runoff water quality and reduce runoff volumes relative to urban systems without SCMs, particularly for small, frequent rain events. Infiltration SCMs include infiltration basins, infiltration trenches, infiltrating rain gardens, and bio-infiltration basins amongst other practices. Unfortunately, infiltration SCMs have a failure rate in the range of 10 to 50 percent (Bean & Dukes, 2016; CTC & Associates LLC, 2018; Hilding, 1994; Lindsey et al., 1992). This failure rate represents a time period where the water quality and water quantity goals are not realized as well as a substantial capital expenditure to remediate the failure. One of the causes contributing to this failure is that the in-situ saturated hydraulic conductivity (K_{sat}) is often not well characterized. Some state jurisdictions allow soil texture to be used as a proxy for in-situ measures of K_{sat} (Minnesota Pollution Control Agency, 2018; Washington State Department of Ecology, 2019; Wisconsin Department of Natural Resources, 2017). However, the variability of K_{sat} within a soil texture group can exceed the variations between soil texture groups (Lee, Traver, & Welker, 2016). Some state jurisdictions allow the in-situ infiltration measurement from a single point to be utilized for design (Minnesota Pollution Control Agency, 2018; North Carolina Department of Environmental Quality, n.d.; Pennsylvania Department of Environmental Protection, 2006). However, soil properties can vary significantly across short distances even within a single soil order (Mulla & McBratney, 2001). Therefore, multiple measurements of K_{sat} are necessary to capture this natural heterogeneity even for relatively small infiltration SCMs (Ahmed et al., 2015; Paus et al., 2014).

Regulating agencies often consider a variety of measurement methods to be acceptable (Minnesota Pollution Control Agency, 2017; Washington State Department of Ecology, 2019). However, there is limited information on the bias associated with each method.

Many factors can influence measured K_{sat} values in the field. Some factors can be controlled or corrected, such as influent temperature. Others present persistent problems that are not easily quantified, such as the influence of anisotropy, depth heterogeneity, or soil structure. Emerson & Traver (2008) found that intra-annual variability of infiltration rate varied by roughly a factor of 2, resulting primarily from temperature-induced viscosity changes of the ponded water. Numerous studies have completed infiltration measurements using various methods, in various land uses, and found the range of measured values often exceeded an order of magnitude within a

distance as short as 1 meter (Asleson et al., 2009; Gupta et al., 2006; Munoz-Carpena, Regalado, Alvares-Benedi, & Bartoli, 2002; Press, 2019; Reynolds, Bowman, Brunke, Drury, & Tan, 2000). The lack of an independent reference standard for which to compare field measured K_{sat} values is perhaps the greatest difficulty in assessing bias of infiltration measurement methods using field sites (Reynolds et al., 2000). It was therefore determined that the bias inherent to each infiltration measurement method could not be isolated from natural variability under field conditions.

There are two primary sources suspected to be contributing to bias in infiltration measurements. For methods that assume 1-dimensional flow, the bias is likely due to the true flow path diverging laterally, creating an overestimation of the true K_{sat}. Alternatively, there are methods that account for the 3-dimensional flow either through an assumed geometry or an empirical correction factor. The source of bias in these methods likely derives from a difference between the assumed and true flow geometries and may either under-estimate or over-estimate the true K_{sat}.

It is proposed to use a numerical solution of the Richards equation to conduct numerical experiments of infiltration for each of the different infiltration methods and thereby remove the unknown natural variability of soils. Values of K_{sat} input to the numerical experiments would serve as an independent reference standard to assess bias. Such numeric simulations have been previously used to successfully evaluate individual infiltration measurement methods (Ahmed et al., 2014; Reynolds, 2010), unique soil conditions (Kindred & Reynolds, 2020), and SCM performance (Sasidharan et al., 2018). The limited scope of these previous studies does not allow for a simple comparison between methods. The objective of this chapter is to use numerical experiments to evaluate the bias of 7 commonly utilized infiltration methods, removing spatial variability and other unknown sources of error associated with field measurements.

Methods

Numerical Solution Procedure

The Subsurface Flow module within the COMSOL Multiphysics 5.4 software package was utilized to implement the finite element solutions ("COMSOL Multiphysics v. 5.4," n.d.). All numerical experiments were time dependent. The variably saturated flow was assumed to be governed by the Richards equation (Richards, 1931). A modified form of the van-Genuchten Mualem soil-water retention function was implemented following (Vogel et al., (2001).

A two-dimensional axisymmetric domain was established for all numerical experiments. Half of each infiltrometer was placed in the domain, corresponding to the axisymmetry. The top boundary outside the infiltrometer and the outer vertical boundary were specified as a no flow condition, and the domain was sufficiently large such that the no flow boundaries did not influence the variably saturated flow from the simulated device. The bottom boundary, representing vertical flow to lower soil stratum, was defined as the unsaturated hydraulic conductivity under a unit hydraulic gradient, i.e., was free draining. The constant head methods were prescribed using a constant pressure head boundary condition in the infiltration device. The falling head methods were specified by determining the cumulative time variable flux across the device boundary, converting it to an equivalent depth, and subtracting this equivalent depth from the initial head applied to the boundary. Rings that penetrated the soil domain were represented using an interior wall boundary condition. Boreholes were represented by removing the area of the borehole from the soil domain, with the appropriate boundary condition applied within the borehole. For uncased boreholes, the pressure head boundary condition was applied as a function of elevation within the borehole. A step function, smoothed to eliminate discontinuities in the first two derivatives, was used to smooth all sharp transitions in boundary conditions, including initialization and rapid changes in head, to allow the solution to converge.

Seven different homogeneous, isotropic soils were specified as input to the simulations. While field soils are heterogeneous and anisotropic, the simplification to a homogeneous and isotropic soil domain provides an unambiguous reference standard to isolate the bias associated with each infiltration measurement method from other factors. The soil water retention characteristics (K_{sat}, α, n, θ_r, θ_s) of each specified soil texture was based on the mean value of each parameter following Carsel & Parrish (1988) and are displayed in Table 3.1. Four different initial soil water pressure head (Hp_0) conditions were defined for each soil texture. For coarse soils, the initial relative soil moisture (Se_0) varied from approximately 20% to 80% in 20% increments. Relative soil moisture (Se) is defined here as the volumetric soil moisture expressed as a percentage between the residual water content (θ_r) and saturated water content (θ_s). Finer textured soils were limited to a maximum initial soil suction head of 10 meters, in increments of 2.5 meters. This was selected as clay soils in natural conditions would retain water and be relatively moist. In all cases, the initial relative soil moisture values covered a range of likely values on the soil-water retention function. A full factorial design was implemented on the infiltration measurement method, soil

texture, and initial soil moisture resulting in a total of 196 simulations (7 infiltration measurement methods, 7 soil textures, and 4 initial soil moistures).

Table 3.1 Soil water retention function parameters associated with each simulated soil texture, based on the mean values from Carsel & Parrish (1988). α is the shape parameter, n is the pore-size distribution parameter, θ_r is the residual water content, θ_s is the saturated water content, H_{p0} is the initial soil water pressure head, and Se_0 is the initial relative soil moisture.

	K_{sat}	α	n	θ_r	θ_s	H_{p0}	Se_0
Soil Texture	(m/s)	(1/m)	(-)	(-)	(-)	(m)	(-)
Sand (S)	8.250E-05	14.5	2.68	0.045	0.43	-0.05	82%
						-0.0752	61%
						-0.1079	41%
						-0.1745	20%
Loamy Sand (LS)	4.053E-05	12.4	2.28	0.057	0.41	-0.0589	82%
						-0.0958	61%
						-0.1499	41%
						-0.2762	20%
Sandy Loam (SL)	1.228E-05	7.5	1.89	0.065	0.41	-0.1023	81%
						-0.1901	61%
						-0.3438	41%
						-0.7985	20%
Sandy Clay Loam (SCL)	3.639E-06	5.9	1.48	0.1	0.39	-0.1682	81%
						-0.42	61%
						-1.0966	41%
						-4.7953	20%
Silt Loam (SiL)	1.250E-06	2	1.41	0.067	0.45	-0.5526	80%
						-1.5184	60%
						-4.5058	40%
						-10	29%
Sandy Clay (SC)	3.333E-07	2.7	1.23	0.1	0.38	-0.7278	80%
						-3.2146	60%
						-7.5	50%
						-10	47%
Silty Clay (SiC)	5.556E-08	0.5	1.09	0.07	0.36	-2.5	93%
						-5	90%
						-7.5	87%
						-10	85%

Infiltration Measurement Methods

A total of 7 infiltration measurement methods were evaluated in this study. These methods were selected as they are either allowed by regulating agencies, well-cited in the literature, or there is interest in adopting the method if it is shown to be reasonably accurate. The infiltration

measurement methods evaluated in this chapter are the double ring infiltrometer (DRI), Saturo by Meter Group (SAT), modified Philip-Dunne Infiltrometer (MPD), Turf-Tec IN2-W infiltrometer (TT), Well Permeameter USBR 7300-89 (WP), Philip-Dunne Permeameter (PD), and Guelph Permeameter (GP). These methods include both constant head and falling head methods. The observed variable for the constant head methods is the time variable flow rate, while the observed variable for the falling head methods is the time variable head. The output from the numerical experiments was post-processed following the procedure described by each method to determine a K_{sat} value. For methods that calculate infiltration rate rather than K_{sat}, the quasi-steady infiltration rate is typically assumed to be equal to K_{sat}. That assumption will be made herein.

The DRI as defined by ASTM International (2018b) is perhaps the most commonly implemented method for measuring infiltration rate. A constant head is maintained in two concentric rings, and the volumetric flow rate is measured in each ring. The volumetric flow rate of the inner ring is used to calculate the value of K_{sat} from the infiltration rate using a 1-dimensional flow assumption. The simulated test soil surface is contained within the 30-cm diameter inner ring, resulting in a horizontal test area of 706.9 cm^2.

The Saturo is a proprietary device that calculates the K_{sat} using a single ring infiltrometer and a dual head calculation procedure (Meter Group, 2019). The dual head procedure utilizes the measured steady state infiltration rate at two different constant head levels. The Saturo documentation recommends 2 cycles of alternating high- and low-pressure head for wet soils, and 3 cycles for dry soils. Three cycles were used for all conditions herein. The recommended total run time varies from 75 minutes to 180 minutes based on soil texture and moisture. The theory supporting the dual head procedure is based on the work of Reynolds & Elrick (1990) and Nimmo, Schmidt, Perkins, & Stock (2009). The Saturo insertion ring has a 14.4 cm diameter, resulting in a horizontal test area of 162.9 cm^2.

The MPD is an ASTM standard single ring falling head device that utilizes an optimization procedure to calculate the K_{sat} and Green-Ampt soil suction head (ASTM International, 2018a). The optimization utilizes the measured time variable head within the single ring, initial and final volumetric soil moisture, Green-Ampt assumptions of a sharp wetting front, and an assumed capped spherical saturation zone geometry. MPD simulations were completed with an initial ponding depth of 30 cm and were terminated when 30 cm of water had infiltrated or a maximum

duration of 24-hours. The MPD utilizes a 10 cm diameter ring, resulting in a horizontal test area of 78.5 cm^2.

The TT is a small, falling head, double ring infiltrometer (Turf-Tec International, n.d.). The TT has historically been used in the turf-management industry. However, the small size, ease of use, and minimal water requirement have generated interest in the TT. The TT uses a time-averaged 1-dimensional flow assumption to calculate the infiltration rate, which is assumed to approach K_{sat}, following an initial wetting period. In this chapter, a 15-minute wetting period and a 15-minute testing period are utilized for all soil conditions as recommended by the Turf-Tec manual, although the user can vary this period based on the observed infiltration rate and user experience. The inner ring of the TT has a diameter of 6.03 cm, resulting in a horizontal test area of 28.6 cm^2.

The WP is a constant head borehole method completed in an uncased borehole (USBR 7300-89, 1989). The WP uses a steady state flow assumption, and an empirical correction for the 3-dimensional flow including lateral flow through the uncased borehole. The WP can be completed with various configurations of well diameter and ponding depth. Following recommendations for a typical configuration, the WP was simulated with a 15 cm diameter borehole (177 cm^2 horizontal area) and a ponding depth of 15 cm.

The PD is a falling-head method implemented in a solid walled borehole (Philip, 1993). A spherical 3-dimensional flow geometry is assumed. The time variable head, initial and final volumetric soil moistures, an assumed spherical flow geometry, and borehole geometry are used to calculate the K_{sat} and soil suction head using an optimization procedure. The PD procedure applied within this chapter utilizes the entire time variable head curve and a trust-region-reflective algorithm within a non-linear least squares regression (MathWorks, n.d.) to optimize the K_{sat} and soil suction head. PD simulations were terminated when 30 cm of water have been infiltrated or a maximum duration of 24-hours. The PD was simulated using a 10 cm diameter borehole (78.5 cm^2 horizontal area), although alternative diameters are possible.

The GP is a proprietary borehole device that calculates K_{sat}, soil sorptivity, and matrix flux potential in an uncased borehole (Soilmoisture Equipment Corp., 2012). The GP can calculate soil properties using either a single head or double head method, depending on the desired accuracy. This chapter will implement the more accurate double head method. The GP was originally described by Reynolds & Elrick (1986). Three-dimensional flow is accounted for by a shape factor that is a function of soil microscopic capillarity length and therefore varies with soil

texture as described by Zhang, Groenevelt, & Parkin (1998). The GP is simulated using a 6 cm diameter borehole (28.3 cm^2 horizontal area), and constant head depths of 10 cm and 20 cm.

Some important characteristics of each of the 7 infiltration measurement methods are summarized in Table 3.2, and an image of each of the 7 infiltration measurement methods is included in Appendix A.

Table 3.2 Comparison of selected infiltration measurement methods. DRI is the double ring infiltrometer, SAT is the Saturo infiltrometer, MPD is the modified Philip-Dunne infiltrometer, TT is the Turf Tech infiltrometer, WP is the well permeameter USBR 7300-89, PD is the Philip-Dunne permeameter and GP is the Guelph Permeameter.

Infiltration Measurement Method	Flow Condition	Test Arrangement	Assumed Dimensionality	Measured Property
DRI	Constant Head	Surface	1-D	Infiltration Rate
SAT	Constant Head	Surface	3-D	K_{sat}
MPD	Falling Head	Surface	3-D	K_{sat}
TT	Falling Head	Surface	1-D	Infiltration Rate
WP	Constant Head	Borehole	3-D	K_{sat}
PD	Falling Head	Borehole	3-D	K_{sat}
GP	Constant Head	Borehole	3-D	K_{sat}

Documented Accuracy of Infiltration Methods

The 7 infiltration methods discussed have varying levels of documentation on their respective accuracy. The DRI and MPD standards both indicate the measures are primarily for comparative use, that many factors influence the tests, and a quantitative statement on precision or bias is not provided (ASTM International, 2018b, 2018a). The Saturo is stated to have an accuracy of +/- 5% with respect to the measured infiltration rate (Meter Group, 2019), and the K_{sat} that is calculated from the infiltration rate at two head levels would have a larger error. The GP states that the single head method can estimate K_{sat} within a factor of 2, and that the two head method is more accurate, but the accuracy of the two head method is not clearly documented (Soilmoisture Equipment Corp., 2012). The TT manual discusses accuracy and variation from lab measures as a result of the TT capturing field conditions such as vegetative cover and in-situ soil properties, but

a quantitative statement regarding accuracy is not made (Turf-Tec International, n.d.). Philip (1993) describes the PD procedure as approximate, although does not quantify the approximation. No statement on the accuracy of the WP could be located. The motivation of this work is to provide a quantitative estimate of the bias associated with each method and allow the relative accuracy to be compared between methods.

Recommended K_{sat} Range for Each Method

The recommended K_{sat} range of each infiltration measurement method was identified, when available. Table 3.3 describes which soils are likely to be well characterized by each infiltration measurement method based on the documentation. Infiltration measurement methods are likely to be less accurate when implemented in a soil with hydraulic properties outside the recommended range.

Table 3.3 Recommended range of K_{sat} for the simulated infiltration measurement methods and simulated soil textures. An "X" and a "-" indicate the soil is within and outside the recommended K_{sat} range of the method, respectively.

Infiltration Measurement Method [recommended K_{sat} range (m/s)]	S	LS	SL	SCL	SiL	SC	SiC
DRI [1e-7 to 1e-4]	X	X	X	X	X	X	-
Saturo [2e-8 to 3e-4][a]	X	X	X	X	X	X	X
MPD [6.9e-7 to 4e-3]	X	X	X	X	X	-	-
TT [4.4e-7 to 3e-4][b]	X	X	X	X	X	-	-
WP [1e-7 to 1e-3]	X	X	X	X	X	X	-
PD [6.9e-7 to 4e-3][c]	X	X	X	X	X	-	-
GP [1e-7 to 1e-4]	X	X	X	X	X	X	-

a) The range of K_{sat} is estimated from the range of infiltration rates, recommended difference in applied pressure head (Meter Group, 2019), and with a quasi-steady state Darcy's Law assumption.

b) Clearly defined minimum and maximum values could not be located within Turf-Tec International (n.d.). The minimum and maximum values were estimated based on the device gradation, range of suggested monitoring durations, and the assumption that quasi-steady state infiltration rate approaches K_{sat}.

c) Clearly defined minimum and maximum values could not be located for the PD within Philip (1993). The minimum and maximum values were based upon values established for the MPD.

Determination of Quasi-Steady State

All numerical experiments completed in this study were for transient conditions, although 4 of the 7 methods utilize a constant head flow condition and a steady state assumption. A transient analysis is implemented to mimic the field measurement methods as closely as possible. Therefore, a criterion for quasi-steady state is required to determine when the method would be terminated if completed in the field. Of the 4 constant head methods, only the Saturo provides specific guidance on the duration of the test. The Saturo simulations were completed for 3 cycles alternating high- and low-pressure head, as recommended for dry soils, for each soil type and initial soil moisture. The GP does not provide a minimum required duration but recommends

monitoring the rate of fall in the supply reservoir until the rate does not change significantly over three consecutive time intervals. The duration of the time intervals may vary from 2 minutes to 15 minutes as the soils vary from coarse to fine. The GP does not clearly, quantitatively define what constitutes a significant change over a time interval. The DRI and WP have a 6-hour minimum duration but recommend extending the test duration if the flow rate has not stabilized. In addition, the WP provides a minimum and maximum volume of water that should be infiltrated, but quantitative guidance on when to terminate the test between these volumes was not located. The guidance on the DRI and WP both refer to continuing the test until a relatively constant flow rate is obtained, but do not provide quantitative guidance on what is sufficiently minimal change. The PD, MPD and TT are falling head methods and therefore do not require an assumption of quasi-steady state.

This chapter will implement a quasi-steady state criterion for the DRI, WP, and GP as a variation of flow of less than 1% over a duration of 15-minutes. The DRI and WP will utilize a minimum test duration of 6 hours. The WP will also utilize the minimum water volume recommended in the method.

Results

The bias is defined as the "measured" K_{sat} determined by the device procedure, divided by the K_{sat} input to the numerical experiment. The "measured" K_{sat} is in quotations to indicate the measurement occurred in a numeric experiment rather than in a physical soil. A sample of the output from the numerical experiments is included in Appendix A. As noted in Table 3.2, the DRI and TT measure infiltration rate rather than the soil property K_{sat}. However, for purposes of comparing methods, the quasi-steady state infiltration rate is assumed to approach K_{sat} as the hydraulic gradient approaches unity. Therefore, a bias of 1 indicates the infiltration measurement method exactly calculated the input K_{sat} value. Bias of less than 1 indicates an underprediction of the input K_{sat}, while bias greater than 1 indicates an overprediction.

Antecedent soil moisture is highly variable spatially and temporally in natural conditions. A dry antecedent soil moisture may require a longer test duration to achieve a steady state condition. Figure 3.1 shows the bias as a function of the initial relative soil moisture for each of the 7 infiltration measurement methods. It is observed that the variation in bias across initial relative soil moisture values within a soil texture class is relatively minimal for most soil textures except the silty clay. This indicates that the test durations are sufficient to allow a quasi-steady state to

develop for the methods implementing a steady-state assumption, and that initial soil moisture is likely not a substantial source of bias. The TT is influenced the most by initial relative soil moisture, most notably in fine textured soils. Tabulated results are provided in Appendix A.

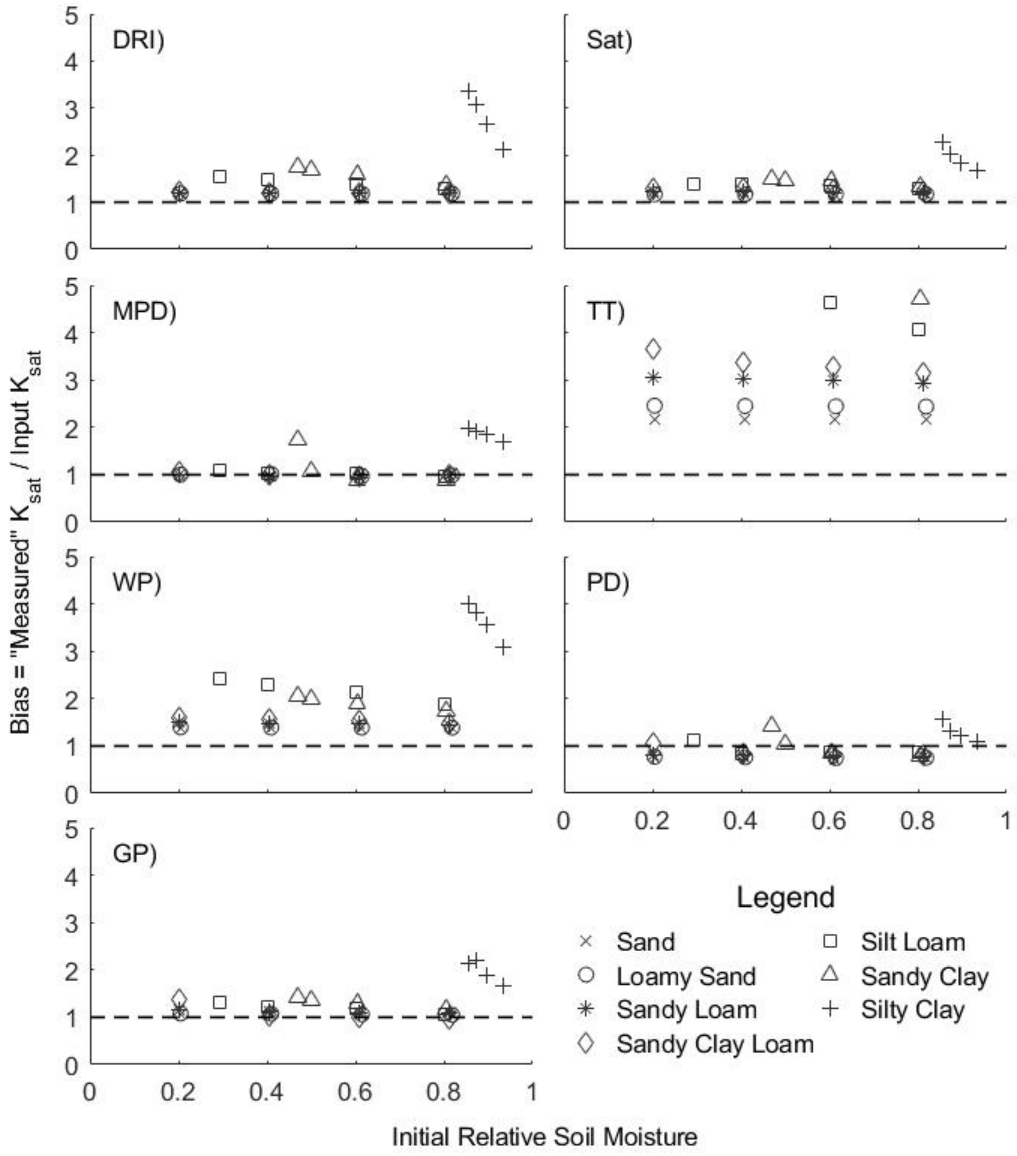

Figure 3.1 Bias as a function of initial soil moisture for each combination of method and soil type. There are silt loam, sandy clay, and silty clay points on the Turf-Tec (TT) sub-plot that exceed the displayed range of bias.

The duration of time required to take a measurement in the field is a metric approximating the difficulty of completing the measurement. Figure 3.2 shows the bias as a function of the duration

of time that the test would be run in the field for each infiltration measurement method and soil texture. Tabulated results are provided in Appendix A.

The duration of time for each method shown in Figure 3.2 follows the criteria chosen to terminate simulations. The quasi-steady state criteria used to terminate the DRI, WP, and GP was discussed previously as a change in flow of less than 1% over a 15-minute period. The MPD and PD were allowed to drain completely which is when the methods should be the most accurate according to Philip (1993). The Saturo was set to complete 3 cycles alternating between a high head and a low head, following an initial soak, although the Saturo manual suggests 2 cycles is sufficient for initially wet soils. The TT was run for 2 consecutive 15-minute intervals as recommended, but this duration can be shortened or extended at the discretion of the user. The duration of time in Figure 3.2 only includes the time when the method is actually infiltrating water, and excludes any time associated with assembly or disassembly in the field. Therefore, the results in Figure 3.2 should be considered comparative rather than an absolute statement on the duration required to complete each method.

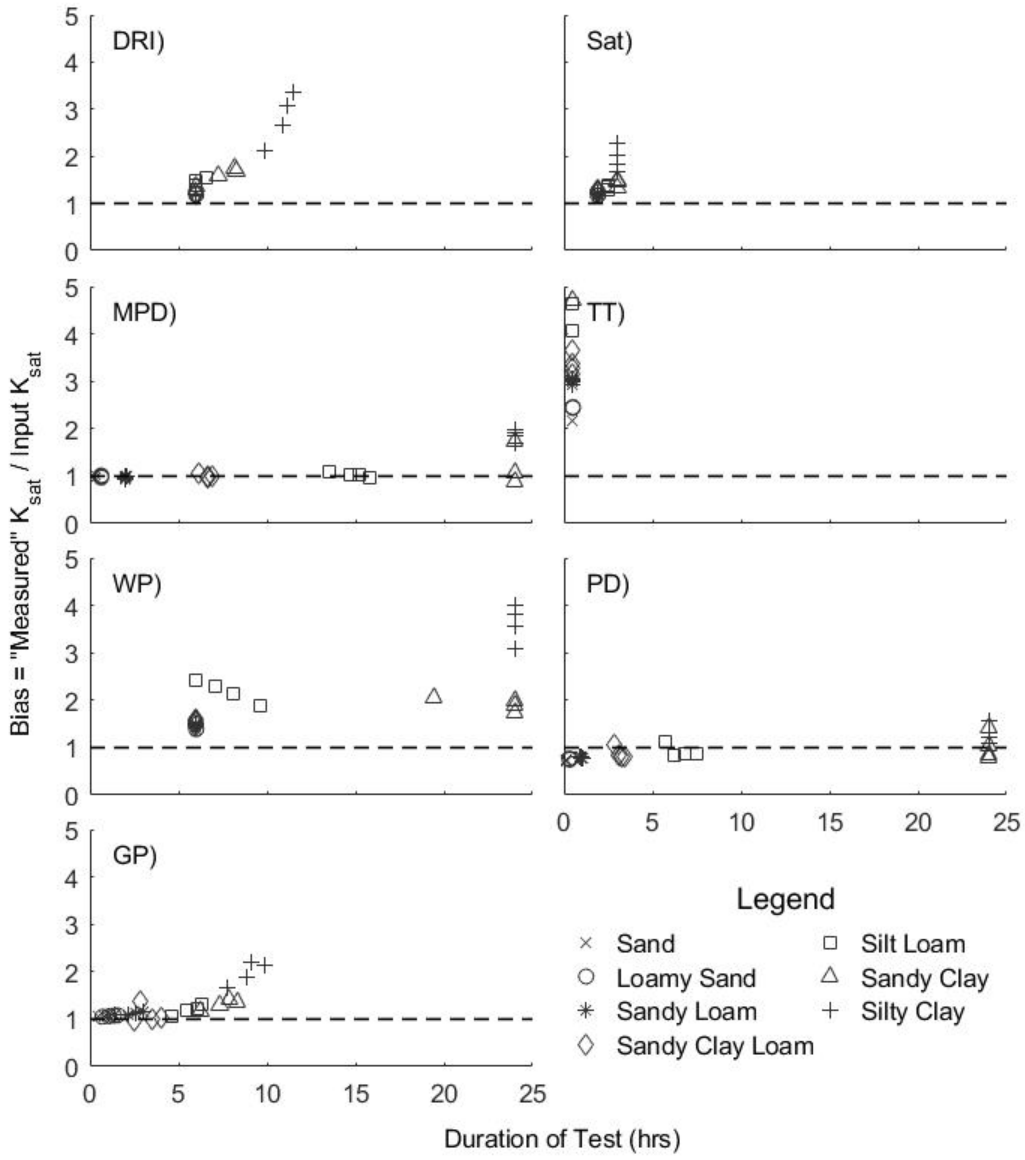

Figure 3.2 Bias as a function of test duration for each combination of method, soil type, and initial soil moisture. There are silt loam, sandy clay, and silty clay points on the Turf-Tec (TT) sub-plot that exceed the displayed range of bias.

As shown in Figure 3.1 and Figure 3.2, the DRI performs consistently for all soil textures within the recommended K_{sat} range of the method. The DRI bias varies between 1.18 and 1.76 for soils sand through sandy clay that are within the recommended K_{sat} range. It is of note that all biases exceed 1 and are therefore non-conservative, in that the SCM will infiltrate below expectations. The DRI documentation (ASTM International, 2018b) does require a minimum test duration of 6

hours and clay texture soils may require a duration in excess of 24 hours to achieve steady state, as shown in Figure 3.2.

The Saturo performed well showing a bias in the range of 1.16 to 1.49 for sands through sandy clay soils. The maximum bias was 2.27 and occurred in a dry, silty clay. The Saturo was a relatively rapid test with durations varying between 115 and 180 minutes for all soil textures.

The MPD both underpredicted and overpredicted K_{sat}, with bias ranging from 0.95 to 1.08 when considering sand through silt loam soils that are within the recommended K_{sat} range of the method. The range of bias increased to 0.88 to 1.96 across all soil textures including those outside the recommended K_{sat} range and when less than the full water depth was infiltrated. The time required to infiltrate 30 cm of water, as shown in Figure 3.2, varied from 19 minutes for the sand to in excess of 24 hours for the clay soil textures. The MPD would be a rapid test for sand and loamy sand soils with test durations less than 45 minutes. It would be less rapid for sandy loam and sandy clay loam soils, with test durations of approximately 2 hours and 6.5 hours, respectively. Arrangements for longer duration tests would be required for silty loam, sandy clay, and silty clay soil textures.

The TT showed the greatest bias of any of the methods evaluated. The variability in the bias across initial soil moisture, within the same soil texture, was relatively minimal for coarse soils where infiltrating SCMs are likely to be constructed. The bias varied between 2.15 and 6.21 for soil textures from sand to silt loam. The maximum bias was 20.28 for the dry, silty clay. Two consecutive 15-minute periods were implemented; therefore, all durations of the test are 30 minutes as shown in Figure 3.2.

The WP had bias ranging from 1.37 to 2.42 for sand through sandy clay soils that are within the recommended K_{sat} range of the method. The maximum bias was 3.98 for the dry, silty clay. The minimum duration of the test is 6 hours. The clay soil textures did not achieve either the quasi-steady state criteria or the minimum volume within the 24-hour simulation.

The PD bias ranged from 0.73 to 1.14 for soil textures in the range from sand through silt loam that are within the recommended K_{sat} range. The full depth of water infiltrated within the maximum 24-hour simulation duration for these soils. The range of bias increased from 0.15 to 1.58 across all soil textures including those outside the recommended K_{sat} range and when less than the full water depth was infiltrated.

The GP had a bias ranging from 0.95 to 1.41 for soils from sand through sandy clay that are within the recommended K_{sat} range. The bias increased to a maximum of 2.2 for the dry, silty clay, that is outside the recommended K_{sat} range. The test duration was relatively rapid ranging from 30 minutes in wet, sandy soils to a maximum of 9.85 hours in dry, silty clay soils.

The DRI, WP, and GP all utilized a quasi-steady state criterion established by the authors to determine when to terminate the simulation. The DRI and WP methods both require a 6-hour minimum duration. The GP two head method does not have a minimum duration, but as the method is completed at 2 head levels and a 15-minute window is required to establish quasi-steady state, 30 minutes is the shortest duration considered herein as illustrated in Figure 3.2. All three methods produce results at earlier times and appear to converge on a steady state more rapidly than the 6-hour minimum duration.

The specified measurement time or volume may not be required for a given accuracy with a given soil. Figure 3.3 shows the bias of the DRI, WP, and GP over the first 6-hours of the simulation. Coarse soils achieve a quasi-steady state much earlier in the test, converging rapidly with little variation between 1 and 6 hours for each method. This may suggest that for coarse, high infiltration rate soils typical of infiltration SCMs, infiltration measurements can be terminated at a shorter duration. In the finer texture soils, the 6-hour minimum seems appropriate and may need to be extended further to reach a quasi-steady state condition. The variation of curvature in the GP time variable bias, displayed in Figure 3.3, corresponds to the differing shape factors associated with the coarse textured soils, i.e. S, LS, and SL, and the finer textured soils, i.e. SCL, SiL, SC, SiC.

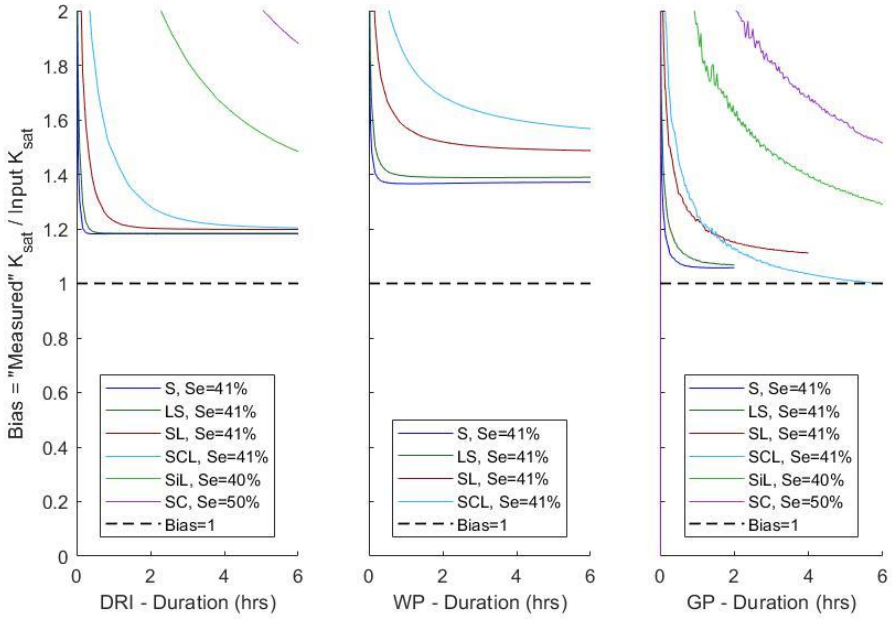

Figure 3.3 Variability of bias as a function of test duration for the DRI, WP and GP. The SiC soil exceeds the displayed range of bias for the DRI and GP plots. SiL, SC, and SiC soils exceed the displayed range of bias for the WP plot.

The Saturo method can produce an estimate of K_{sat} as soon as an infiltration rate is measured at each of the two head levels. As simulated, the Saturo method completed 3 cycles alternating between high head and low head, following the initial soak period. Figure 3.4 shows the variability of bias in response to the alternating head cycles over the simulation period for the Saturo. The general trend had the greatest bias at the beginning of a cycle, then it improved as the head was maintained and the infiltration rate stabilized. Later cycles tended to converge more rapidly than earlier cycles. The coarse soils showed minimal variability of bias, suggesting the Saturo provides relatively accurate results early in the simulation period. Finer soils do appear to require the full recommended duration to achieve a reasonable result. The silt loam, sandy clay, and silty clay soils have a bias less than 1 during the first high head cycle, as shown in Figure 3.4. This is a result of the initial infiltration rate during the soak period being high, and the infiltration rate during the first high head cycle stabilizing to a lower infiltration rate than during the low head soak period. The clay soils calculated higher bias during the low head cycles than the high head cycles. This is likely caused by the time required for the soil water pressure at the boundary to return to the low level. The bias is only calculated when the soil water pressure on the

boundary is equal to the applied water pressure, which resulted in the bias being calculated for less than the full low head cycle for the silty clay.

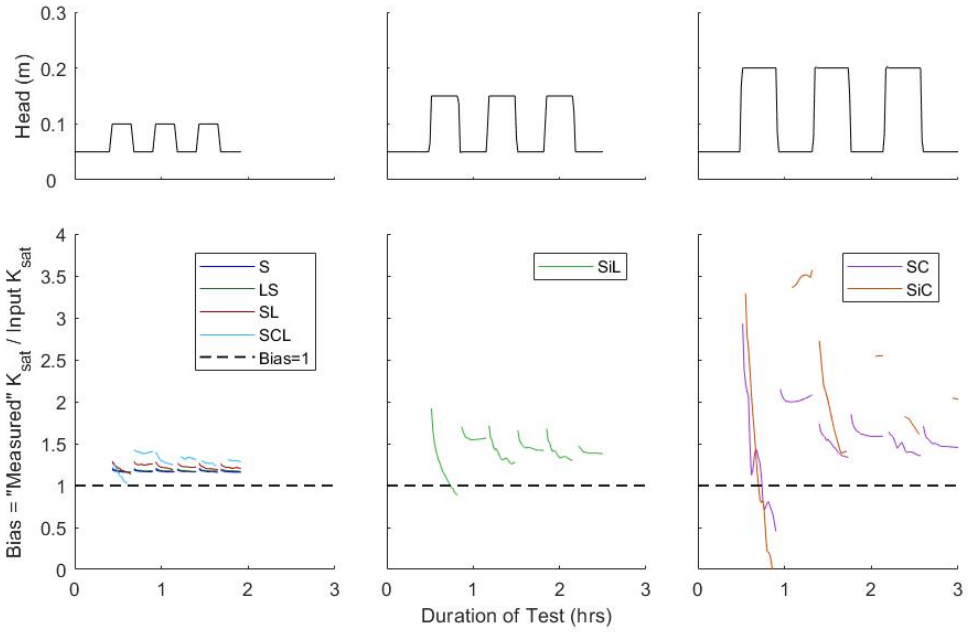

Figure 3.4 Variability of bias as a function of test duration for the Saturo. The K_{sat} is not calculated until an infiltration rate is available at both head levels. The Saturo cycles between 2 head levels as shown in the upper plots. The K_{sat} is not calculated during the transition between head levels. Discontinuities in the lines of a given soil texture occur at the change of head on the Saturo.

As noted by Philip (1993), the PD, and by extension the MPD, are expected to produce the most accurate results when the cylinder is allowed to drain completely. However, the optimization procedure can be completed on a partial time series if a test is terminated prior to the cylinder draining completely. Figure 3.5 shows the bias as a function of the proportion of the cylinder allowed to infiltrate up to the cylinder draining completely. For both methods and across all soil textures, it appears the results are most accurate if at least 50% to 75%, depending upon soil texture, of the initial water volume in the cylinder is infiltrated, in this instance approximately 15 cm to 22.5 cm of the 30 cm initial depth. Philip (1993) notes that the assumed spherical geometry does not hold in the limit of small time, and therefore the reduced accuracy is to be expected when the volume infiltrated is less than the maximum for both the PD and MPD, as observed in Figure 3.5. The PD and MPD drained completely in as little as 9 minutes and 19 minutes, respectively, for a dry sand representing a rapid method of estimating K_{sat}.

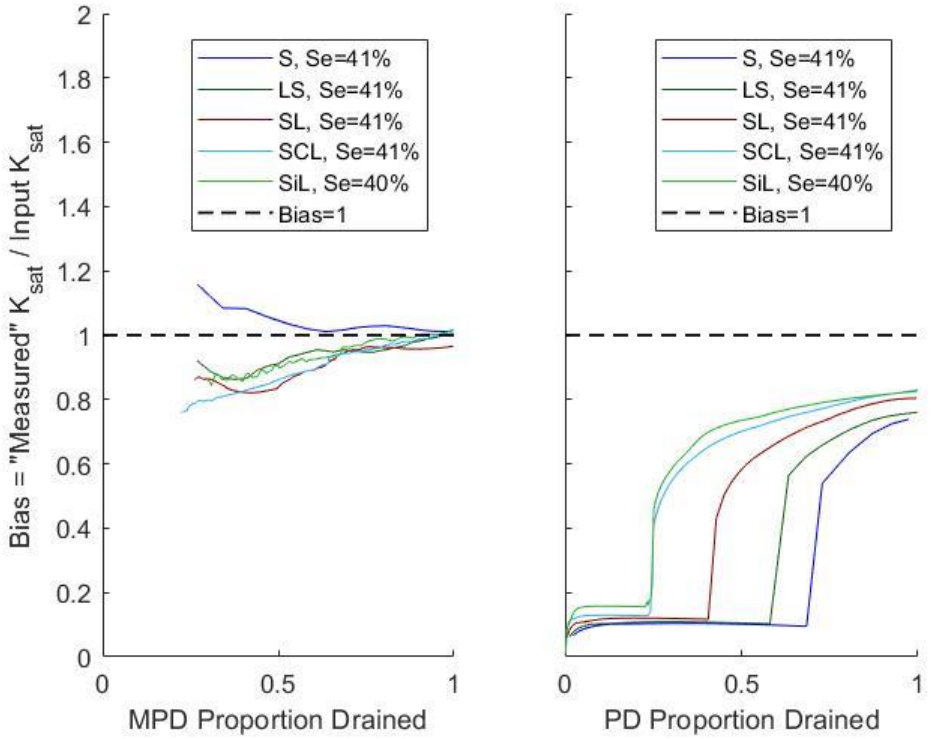

Figure 3.5 Variability of bias as a function of the proportion of the cylinder drained for the MPD and PD. SC and SiC soils did not drain completely within 24 hours and are therefore not plotted. The MPD procedure requires the assumed capped spherical saturation zone to achieve a minimum radius and the optimization does not calculate a value prior to this minimum radius being achieved. Discontinuities in the slope of lines represent a shift in the optimization result.

The TT simulation included a 15-minute pre-soak period, followed by a 15-minute testing period. In the case of the sand, the rings drained completely in less than 15 minutes. Figure 3.6 shows the variability in bias over the pre-soak period and the testing period. In the testing period, the bias is relatively stable after several minutes, except for the SC and SiC soil, implying the pre-soak and testing intervals are of sufficient duration for coarser soil. The bias may be reduced in the SC and SiC soils by extending the pre-soak period and testing period or adding additional testing periods.

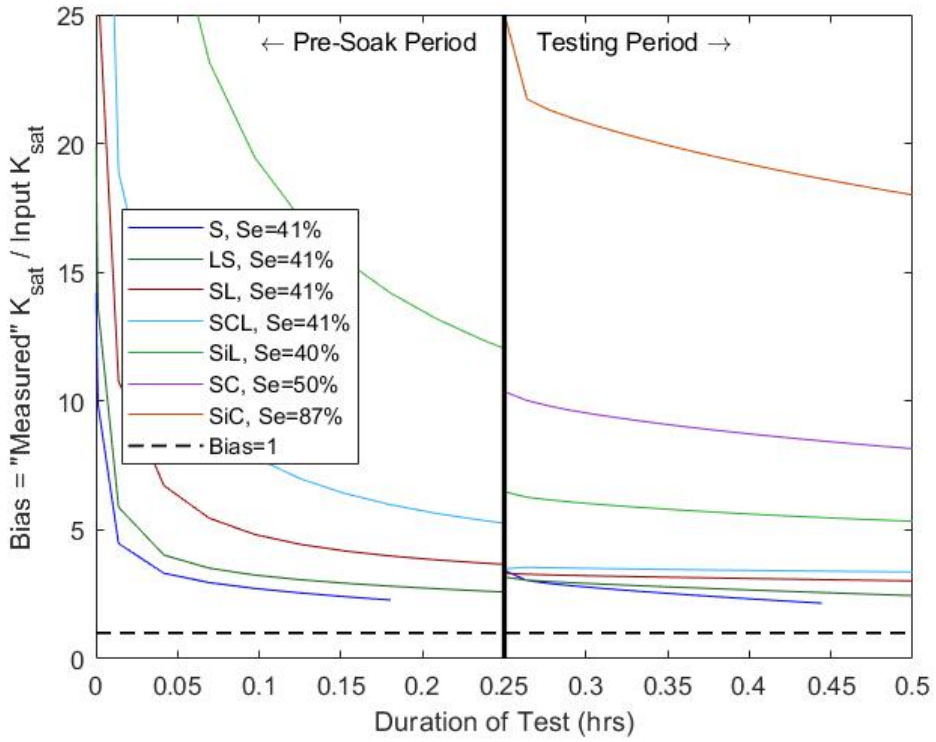

Figure 3.6 Variability of bias as a function of the test duration for the TT. The infiltration rate is not calculated during the step transition to refill the rings for the second 15-minute interval, displayed as a vertical black line. The pre-soak period and testing period are to the left and right, respectively, of the vertical black line. The SC and SiC curves exceed the plotted bias limits during the pre-soak period.

Discussion

One-Dimensional Flow Assumption

The DRI and TT both rely on a one-dimensional vertical flow assumption in the inner ring of the device. The goal of the outer ring is to buffer the divergent flow caused by the soil suction head in the adjacent unsaturated soil, allowing the inner ring flow to be purely vertical. Evaluating the flow net shows that while the flow in the outer ring is more divergent than the inner ring, the flow in the inner ring of both the DRI and TT is laterally divergent. The effect is greater in the TT than the DRI, as the TT has a smaller size and thus the lateral divergence accounts for a larger percentage of the infiltrated water.

Previous studies have indicated that larger diameter double ring configurations can provide reasonably accurate results. In a study on canal seepage where low infiltration rates would be anticipated, Robinson & Rohwer (1957) found that nested rings of 183 cm (6 feet) diameter and 549 cm (18 feet) diameter provided an accurate method of estimating infiltration rate. Lai & Ren (2007) found that a DRI with inner ring of 80 cm and an outer ring of 100 cm reliably estimated K_{sat} in sandy loam, silt loam, and silt soil textures. The diameter of the inner ring, the ratio of the outer ring diameter to inner ring diameter, the ring penetration depth, and the soil texture all influence the assumption of one-dimensional flow. A larger diameter inner ring is less susceptible to divergent flow, as the divergence would represent a proportionally smaller fraction of the total flow. A greater ratio of the outer ring diameter to the inner ring diameter would also decrease the bias, as the outer ring is increasingly able to buffer the background soil suction head. The rings provide a physical barrier to divergent flow while the water is within the soil column contained within the ring, thus a greater penetration depth forces one-dimensional flow over a greater depth of soil. Finer and drier soils have a greater potential soil suction head, and therefore the bias would be expected to be larger as the texture transitions from coarse to fine and the initial soil moisture from wet to dry.

Johnson (1963) provides an early reference to the DRI configuration, including the 30 cm and 60 cm ring diameters and 15 cm penetration depth, now standardized in ASTM International (2018b). The author notes that divergent flow will influence measured infiltration rates, and states the proposed method is versatile and useful when considering economic limitations of larger tests. ASTM International (2018b) also likely considers the physical difficulty of installing larger rings. The preferred DRI installation method recommends using a jack under a truck which is not practical for infiltration SCMs where driving on the soil surface is to be avoided.

Three-Dimensional Flow Corrections

The methods that implement a correction to account for the laterally divergent three-dimensional flow rely on either an assumed geometry or a factor that corrects for the divergent flow paths. The PD uses an assumed spherical flow geometry, while the MPD uses an assumed capped spherical flow geometry. The SAT uses a factor that is a function of the insertion ring diameter and penetration depth. The WP uses a factor that is a function of ponded head, borehole radius, and the steady state flow rate corrected to a standard water temperature. The GP uses a shape factor that is a function of the ponded head, borehole radius, and microscopic capillarity length

following Zhang et al., (1998). The source of bias in these methods is likely due to the true flow path diverging from the simplifying assumptions of the method.

Philip (1993) discusses the idealized flow geometry as being more hydraulically efficient than the in-situ flow path. A factor of $8/\pi^2$ is introduced in the PD formulation, and subsequently the MPD, to account for this excess hydraulic efficiency. It is also of note that coarse soils are more likely to have flow that is dominated by gravity flow and have a larger vertical component, while finer soils likely have higher soil capillarity and therefore more lateral flow. This difference in flow geometry with soil texture likely introduces bias in methods that do not account for the variation and may either under-estimate or over-estimate K_{sat}.

Limitations

Numerical experiments are at best a representation of reality, but always deviate from the in-situ characteristics. The simulated domain was specified as isotropic and homogeneous to provide an unambiguous reference standard; however, this condition almost never exists in nature. The simulations did not account for any soil structure, which can substantially influence the subsurface movement of water. The simulated domains also did not include any type of soil layering, which may result in different results in terms of bias.

The numerical experiments did not account for potentially imperfect implementation of the field procedures. Ring devices and borehole devices assume a tight seal is achieved with the soil interface, and a preferential flow path may exist if the seal is not sufficient. Borehole methods utilize an assumed geometry that may not be identical to the true borehole geometry and smearing of the soil may artificially decrease infiltration rates at the soil water interface. The application of water can suspend fines into the water column, which can clog open pore space, artificially reducing the measured infiltration potential. The sensitivity of specific types of sensors to detect small or large changes in water depth or flow rate was not evaluated. Long duration tests with ponded water may be influenced by evaporation which was not included in the simulations. Finally, water temperature is important in evaluation the infiltration rate of soil (Emerson & Traver, 2008).

With these limitations in mind, the numerical experiments completed should be considered an idealized implementation of each method that allow for relative comparisons between methods. As the discussed limitations could result in either under- or over-estimation, there is not likely a

simple correction that can be applied to account for the various sources of natural variability and random error across all potential situations.

Conclusions

There are many different methods to estimate soil hydraulic properties. When considering the soil where most infiltrating SCMs are located, that is sand through silt loam, the simulated methods had a bias in the range of 0.7 to 6.2. Methods that rely on a 1-dimensional flow assumption, including the DRI, consistently overestimate the infiltration rate. The TT was the only method where the bias exceeded 2.5 for soils from sand through silt loam. The range of bias appears to be reasonable given the natural heterogeneity of soil, but a correction should be considered, particularly for the TT, for engineering applications since a non-conservative error may otherwise be introduced.

All the infiltration measurement methods evaluated herein test a relatively small volume of soil. For many applications including infiltration SCMs, the soil properties need to be characterized over a much larger spatial extent than can be approximated by a single test. Multiple measurements are required to characterize the spatial heterogeneity of infiltration potential when the area of interest exceeds the extent of the tested soil volume (Ahmed et al., 2015). Methods that require less time and less water to estimate K_{sat} may be preferred to the conventional standard represented by the DRI.

When designing infiltration SCMs, it is important to understand the in-situ soil properties over the soil profile. Borehole methods of estimating hydraulic properties allow measurements to be completed at depth without expensive over-excavation. The three simulated borehole methods (i.e. WP, PD, and GP) produced results with similar levels of accuracy to the surface application methods and may be useful in characterizing vertical variations in K_{sat}.

The DRI and WP rely on a steady-state assumption and have a minimum test duration of 6 hours. As noted in Figure 3.3, the DRI and WP reach a quasi-steady state prior to this minimum in many coarse materials. The Saturo, MPD, PD, GP all produce results of comparable accuracy to the DRI and WP, often with a shorter required duration. Selecting a test with a long duration or large water volume does not necessarily increase the accuracy of the measurement.

The TT produced the largest bias of the simulated methods. The range of bias was 2.15 to 6.21 for soil textures from sand to silt loam. However, the variability of K_{sat} between texture classes is

often a factor of 5 to 10. This would suggest that the TT may be useful for differentiating between areas with high and low infiltration potential. The TT may be useful in applications where a rapid field test is required such as construction quality assurance applications, particularly when the surface being tested is known to be a coarse material. A correction factor in the range of 3 to 6 may be appropriate for soil materials in the range of sand to silt loam. For example, García-Serrana, Gulliver, & Nieber (2018) found good simulation of swales after reducing the TT K_{sat} by a factor of 4.3, based upon field comparison measurements taken by J. Houle (personal communication, 2017). The short duration and minimal water volume requirement of the TT test may allow for a large number of tests, corrected for bias, to be completed to characterize the variability of infiltration rate over an area.

The Saturo, MPD, PD, and GP were the most accurate methods for the silty clay soil texture. However, the MPD, PD, and GP require a substantially longer duration of test than the Saturo for fine soils, as shown in Figure 3.2. For coarser soils, the MPD, PD and GP produce relatively accurate results with lower duration. The Saturo appears to be able to estimate the K_{sat} within a factor of 2.3 or less and with a duration of 3 hours or less, which may be very useful when exploring areas with limited knowledge of the soil characteristics.

Chapter 4 Spatial Correlation of Field Saturated Hydraulic Conductivity

Summary

Field saturated hydraulic conductivity (K_{fs}) is an important parameter influencing local hydrology and is the limiting soil parameter in urban systems that are attempting to promote the natural processes of stormwater infiltration and evapotranspiration. However, poor characterization of K_{fs} may result in a misunderstanding of the local hydrology and failure of infiltration stormwater control measures (SCMs). Geostatistics will be utilized to investigate the spatial correlation of K_{fs} in developed, urban systems, including infiltration SCMs, where the sampled soil volume was placed by construction equipment rather than natural geologic processes. K_{fs} was measured at 9 sites using a modified Philip-Dunne infiltrometer. The sites include 3 rain gardens, 3 turf grass park areas, and 3 grass swales. All sites measured K_{fs} spanning multiple orders of magnitude. Inspection of the magnitude of K_{fs} would indicate that all sites have reasonable infiltration potential. Variograms of the surface K_{fs}, assuming the soil was horizontally isotropic, were constructed for each site to evaluate the spatial correlation range, i.e. the distance when measurements become spatially independent. Two of the nine sites showed spatial correlation and theoretical variograms were fit to the experimental data. The spatial correlation range was calculated to be 7.9 meters and 22.9 meters at these sites. The other seven of the sites showed a relatively flat pattern in the variogram indicating a lack of spatial correlation, referred to as a pure nugget effect. For a property that is known to have spatial dependence like K_{fs}, a pure nugget effect often indicates the spatial dependence occurs at a separation distance less than the sample spacing. The spatial correlation range for the sites exhibiting pure nugget effect is less than the sample spacing varying from less than 1 meter to less than 7.4 meters. Therefore, the spatial correlation range typical of K_{fs} in disturbed urban systems may vary from less than 1.0 meter to 22.7 meters, with most sites having a spatial correlation range less than 5 meters. The observed spatial correlation range of K_{fs} in this study appear to be towards the lower end of the range observed in other studies. This would seem reasonable as the soil at all sites were disturbed by excavation, import of fill, compaction, vehicle traffic, variable stormwater loading, vegetation lifecycles, and human activities resulting in a disconnection from the site's quaternary geology and thus a reduction in the spatial correlation length. A fine sample spacing may be necessary if

geostatistics are utilized to characterize K_{fs} in disturbed urban systems. Statistics that assume sampling independence may be a practical method to characterize K_{fs}, but also require a large sample size to reduce the margin of error to an acceptable level. The observed variability over relatively small spatial extents indicate the importance of an adequate number of point measurements to allow for statistically significant results to characterize K_{fs}.

Introduction

The field saturated hydraulic conductivity (K_{fs}) is an important parameter influencing local hydrology as it has a significant influence on the partitioning of rainfall into surface runoff and infiltrated water. The field saturated hydraulic conductivity (K_{fs}) is defined as the measured in-situ saturated hydraulic conductivity (K_{sat}) that is influenced by the soil structure. K_{fs} is a highly heterogeneous soil property that can be time-consuming to estimate but can have substantial influence on the design and performance of stormwater infrastructure as well as the evaluation of hydrologic events.

Green Infrastructure (GI) is a system of practices that attempts to treat stormwater at its source by promoting the natural processes of infiltration and evapotranspiration (U.S. Environmental Protection Agency, 2020). GI includes non-structural practices like minimizing disturbance and conserving green space as well as structural practices such as infiltration basins, bioinfiltration rain gardens, grassed swales, infiltration trenches, and similar stormwater control measures (SCMs). It is often assumed that an increase in pervious surfaces, or directing stormwater to pervious surfaces, will result in reduced surface runoff and reduced surface water pollutant loading. However, the K_{fs} of the pervious surfaces is critical to the in-situ performance as it is the limiting parameter controlling the rate that stormwater can infiltrate to the subsurface.

Many jurisdictions allow a limited number of infiltration measurements to be utilized to characterize infiltration rates for engineering purposes (Minnesota Pollution Control Agency, 2018; Wisconsin Department of Natural Resources, 2017), possibly due to the difficulty and expense involved in completing in-situ K_{fs} measurements. Utilizing a limited number of infiltration measurements in an engineering design assumes that the soil property will be relatively homogeneous. However, variations in composition or disturbance can result in variable K_{fs} over small separation distances. The causes of disturbance may include excavation, import of fill, compaction, vehicle traffic, variable stormwater loading, vegetation lifecycles, and human

activities. The poor characterization of K_{fs} may result in mischaracterization of local hydrology and failure of infiltration SCMs.

Geostatistics have been used in many applications to assess the spatial dependence of various parameters. Soil properties typically have spatial dependence due to the geologic history of the site. The scale of a study is important for interpreting the identified spatial correlation. In geostatistics the scale is composed of the extents (area of sampling domain), spacing (distance between measurements), and support (surface area of measurement) (Blöschl & Sivapalan, 1995). Sampling completed with a large support area results in bulk averaging of the soil parameter and less variance between measures than smaller support areas. Sampling patterns completed with large spacing may indicate spatial correlation at the watershed scale as a result of quaternary geology but miss the spatial correlation related to local disturbances. Gajem, Warrick, & Myers (1981) measured eleven soil parameters at spacings of 20-cm, 200-cm, and 2000-cm along transects in an agricultural field and found the spatial correlation range, the distance when measurements become spatially independent, increased with increasing sample spacing.

This study will investigate the spatial correlation of K_{fs} in developed, urban systems typical of post construction GI practices, including SCMs where the sampled soil volume was placed by construction equipment rather than formed by natural geologic processes. The spatial correlation structure is expected to be dominated by the history of site disturbance including excavation, import of fill, compaction, vehicle traffic, variable stormwater loading, vegetation lifecycles, and human activities. Few studies were identified that evaluated the spatial correlation of K_{fs} at the local scale. No study has been identified that specifically investigated the spatial correlation of K_{fs} at the scale of infiltration SCMs in urbanized areas. Appropriate characterization of K_{fs} can improve the design of infiltration SCMs. An understanding of the spatial correlation structure can be utilized to develop sampling plans that adequately characterize disturbed urban soils. The local hydrology including impacts on flood mitigation and surface runoff quality can be better understood if the K_{fs} of GI is representative of the in-situ condition.

Methods

Field Sites

Field measurements were completed at various areas including infiltration SCMs located in Minnesota, USA. The field site areas include rain gardens, turf grass park areas, and grass swales.

All sites were in developed areas, which is commonly where infiltration SCMs are constructed. Asleson, Nestingen, Gulliver, Hozalski, & Nieber (2009) measured the K_{fs} of 12 rain gardens in 2006. The subset of 3 rain gardens included herein was selected based on having an adequate total number of measurements to allow a variogram to be constructed. Olson, Gulliver, Nieber, & Kayhanian (2013) measured the K_{fs} of the turf grass park areas in 2008. The K_{fs} was also measured by the authors in grass swales in the fall of 2019 and fall of 2020. Table 4.1 compares the sites where K_{fs} was measured. The rain gardens and grass swales are constructed systems and therefore the soil was disturbed by design. The turf grass park areas were selected by the original authors to evaluate methods to remediate compaction and therefore the soil was known to be disturbed.

Table 4.1 Summary of measurement sites

Site Name	GI practice	Year of Measurements	Extent of Measurements
Thompson Lake	Rain Garden	2006	34 m by 11 m
UMN Duluth	Rain Garden	2006	56 m by 38 m
UMN St. Paul	Rain Garden	2006	12 m by 5 m
French Park	Turf grass	2008	40 m by 40 m
Minnetonka Park	Turf grass	2008	44 m by 36 m
Maple Lakes Park	Turf grass	2008	24 m by 20 m
I-94	Grass Swale	2019	214 m by 8 m
TH-8	Grass Swale	2020	290 m by 10 m
TH-212	Grass Swale	2020	480 m by 12 m

Modified Philip-Dunne Infiltrometer

The modified Philip-Dunne (MPD) infiltrometer was utilized to measure the K_{fs} at all sites. The MPD is a 10-cm diameter single ring falling head device described by Ahmed, Nestingen, Nieber, Gulliver, & Hozalski (2014) and standardized in ASTM International (2018). The MPD is a surface infiltrometer that estimates the K_{fs} in approximately the top 30 cm of soil. The MPD

procedure assumes a capped spherical zone of saturation beneath the single ring and a sharp wetting front following Green-Ampt assumptions. The K_{fs} and wetting front suction head are calculated using an optimization procedure on the time variable head, the change in volumetric soil moisture, and the MPD geometry. The flow transitions from one dimensional to three dimensional after the wetting front passes below the penetration depth of the ring. The flow is assumed to be fully three dimensional after a minimum radius of the zone of saturation is achieved, which is based on the penetration depth and cylinder radius. The MPD optimization procedure utilizes the portion of the time dependent head curve where the flow is fully three dimensional.

In the evaluation of the grass swales, the MPD cylinders were allowed to drain up to a duration of 1.5 hours, at which time tests were terminated. At 6 points in the TH-212 grassed swale, the minimum radius criteria were not satisfied and the MPD optimization could not be completed. For these measurements, the K_{fs} was estimated using a 1-dimensional Green-Ampt procedure following Philip (1992). For 1 point in each of the 3 rain gardens, no noticeable drop was observed in the cylinders after several hours and the K_{fs} at these points was reported at 2.5×10^{-3} cm/hr by the original authors.

Variograms

The variogram is a common geostatistical tool used to analyze spatial correlation structure. The variogram plots the variance at various separation distances as a function of those separation distances. A dataset with strong spatial correlation would show a small variance at small separation distances, with the variance approaching the sample variance (s^2) at large separation distances. The variance $\hat{\gamma}(h)$ at separation distance h is estimated by Equation 4.1.

Equation 4.1

$$\hat{\gamma}(h) = \frac{1}{2n(h)} \sum_{i=1}^{n(h)} [z(x_i) - z(x_i + h)]^2$$

The variables $z(x_i)$ and $z(x_i+h)$ are the measured values at a point x_i and a point a distance h away. The variable $n(h)$ refers to the number of data pairs at a separation distance h.

The procedure utilized herein consisted of the smallest bins that would maintain a minimum of approximately 30 to 50 pairs per bin. The separation distance was calculated as the mean

separation distance of pairs within the bin. All values of K_{fs} were log-transformed prior to estimating the variogram. The variance at each separation distance was normalized by the sample variance (s^2) of all points at the site to allow comparison between sites with different magnitudes of K_{fs}. The maximum separation distance included in the variogram was half the greatest distance across the measurement extents to avoid edge effects and ensure an adequate number of data pairs in each bin.

The variogram has several key features including the nugget, sill, and spatial correlation range (range). The nugget is the variance at a separation distance of zero. Theoretically the variance at zero separation distance should be zero, but a non-zero nugget is common and represents sources of error including sampling, measurement, or other unexplained errors. The sill represents the variance at large separation distances. The range is the separation distance at which the measurements become spatially independent. An example variogram showing a pattern indicative of spatial correlation is displayed in Figure 4.1.Variograms where the nugget approaches the sill and the trend in variance is approximately horizontal across the evaluated separation distances are indicative of a lack of spatial dependence and are referred to as a pure nugget effect.

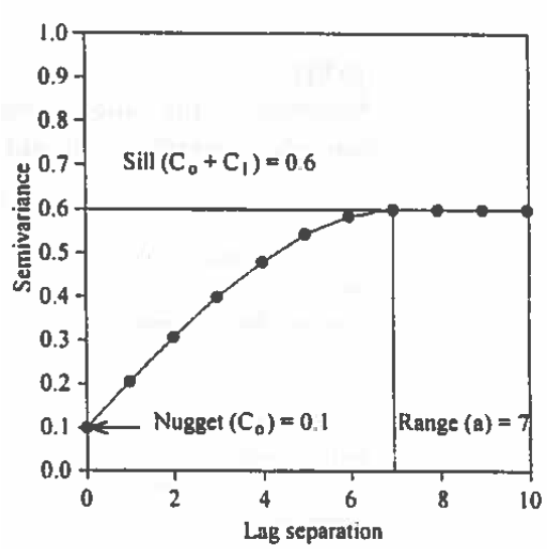

Figure 4.1 Example variogram showing spatial correlation from Mulla & McBratney (2001)

The presence of outliers in the log transformed dataset was investigated using the median of all absolute deviations (MAD) from the sample median (Rousseeuw, 1990). This procedure was selected as it is robust estimator of scale. Outliers were identified if the z-score exceeded an absolute value of 3, corresponding to inclusion of approximately 99.7% of the data assuming a

log-normal distribution. The outliers were removed as their presence in datasets with a small sample size can obscure the spatial structure. This influence is magnified when the physical location of the outlier disproportionately contributes to a limited portion of the variogram, such as when the measurement is near the edge of the sampling extents. The analysis completed herein was also completed on the full dataset, inclusive of outliers, and is included in Appendix B.

All experimental variograms were constructed using data collected at the soil surface and were assumed to be horizontally isotropic. A theoretical variogram was fit to the experimental, isotropic variogram using a weighted least squares optimization procedure (Schwanghart, 2021). The weighting is based on the number of observations, the experimental variance at each separation distance, and the theoretical variance at each separation distance following McBratney & Webster (1986). The theoretical variogram models evaluated were circular, spherical, pentaspherical, and exponential. These theoretical variograms were selected as they are authorized models in two dimensions and frequently used in the literature (Olea, 2006; Webster & Oliver, 2007). The theoretical variogram with the highest coefficient of determination (r^2) value was selected as the best fit. Theoretical variograms were only fit to experimental variograms that visually approximated the shape of the theoretical variogram models (Webster & Oliver, 2007), that is theoretical variograms were not fit to experimental variograms that displayed a pure nugget effect.

Results and Discussion

Table 4.2 displays the descriptive statistics of the K_{fs} measurements at each of the 9 sites. All sites include K_{fs} measurements spanning multiple orders of magnitude. Inspection of the arithmetic mean and standard deviation show that the standard deviation often approaches or exceeds the arithmetic mean. Since negative values of K_{fs} are not possible, this indicates that a normal distribution may not be appropriate. The geometric mean is a more appropriate measure of central tendency for log-normal variables. The multiplicative geometric standard deviation is also provided (Kirkwood, 1979). Maple Lakes Park has the lowest geometric standard deviation with a value of 1.8 indicating a high level of spread at all sites.

Inspection of the arithmetic and geometric means indicate that all sites have reasonable infiltration potential and would infiltrate some stormwater during rain events. Of the 9 sites, only the 3 rain gardens were designed specifically to infiltrate water. The turf grass park areas were designed to be open park space, without stormwater run-on from any adjacent areas. The grassed

swales were primarily designed for conveyance of water rather than infiltration of water. However, the geometric mean K_{fs} at I-94, TH-8, and French Park is approaching or exceeding the K_{fs} of the rain gardens. This would indicate that all nine sites are actively infiltrating stormwater.

Relative frequency histograms, plotted on a log-scale and spanning multiple orders of magnitude, are displayed for all sites in Figure 4.2. Several of the sites visually approach a log-normal distribution, while several of the sites appear slightly skewed.

Experimental variograms are plotted for all sites in Figure 4.3. The variance at each separation distance is normalized by the sample variance of the site. A variogram with spatial correlation would have a small value at small separation distances, then approach 1 as the variance at large separation distances approaches the sample variance and the point measures become spatially independent. The amount of scatter observed in the experimental variograms in Figure 4.3 is inversely proportional to the sample size in Table 4.2 and the number of pairs per bin as shown in Table 4.3. Only the variograms for French Park and Maple Lakes Park show a structure indicative of spatial dependence. Theoretical variograms, fit to the French Park and Maple Lakes Park sites, are described in Table 4.3. The circular variogram model had the highest coefficient of determination for both sites and are plotted with the experimental data in Figure 4.3. The theoretical variograms have a spatial correlation range of 22.7 meters and 7.9 meters for French Park and Maple Lakes Park, respectively. The spatial correlation range is likely due to a change in soil texture, structure, or compaction.

Cambardella et al. (1994) suggests a nugget to sill ratio (N/S) less than 25% indicates strong spatial dependence, N/S between 25%-75% indicates moderate spatial dependence, and N/S greater than 75% indicates a weak spatial dependence. Both French Park and Maple Lakes Park show a moderate spatial dependence with N/S ratios of 0.40 and 0.65, respectively.

The other seven sites all show a relatively flat pattern in the variogram indicative of a pure nugget effect. The pure nugget effect does not mean that a spatial correlation does not exist, but that the sample spacing was too coarse to capture the spatial correlation. Table 4.3 includes the minimum separation distance used in the binning, and it is assumed that the spatial correlation range is less than this value for all sites displaying a pure nugget effect. Therefore, the spatial correlation range for sites exhibiting a pure nugget effect vary from less than 1.0 meters at the UMN St. Paul rain garden to less than 7.4 meters at TH-8 grassed swale.

Table 4.2 Descriptive statistics for evaluated sites

	Count (-)	Arithmetic Mean (cm/hr)	Standard Deviation (cm/hr)	Geometric Mean (cm/hr)	Geometric Standard Deviation (-)	Minimum (cm/hr)	Maximum (cm/hr)
Thompson Lake	28	46.6	54.0	18.0	6.0	0.11	194.6
UMN Duluth	31	21.5	34.2	7.9	4.1	0.50	125.4
UMN St. Paul	38	16.0	13.8	10.9	2.6	1.12	54.5
French Park	144	18.4	31.1	7.3	4.0	0.19	218.2
Minnetonka Park	130	8.2	13.6	3.1	4.1	0.12	80.2
Maple Lakes Park	101	2.3	1.6	1.9	1.8	0.45	9.2
I-94	50	28.1	27.9	16.3	3.2	0.97	114.0
TH-8	36	57.1	73.6	26.0	4.1	0.74	271.7
TH-212	47	18.5	37.1	2.8	11.9	0.004	204.4

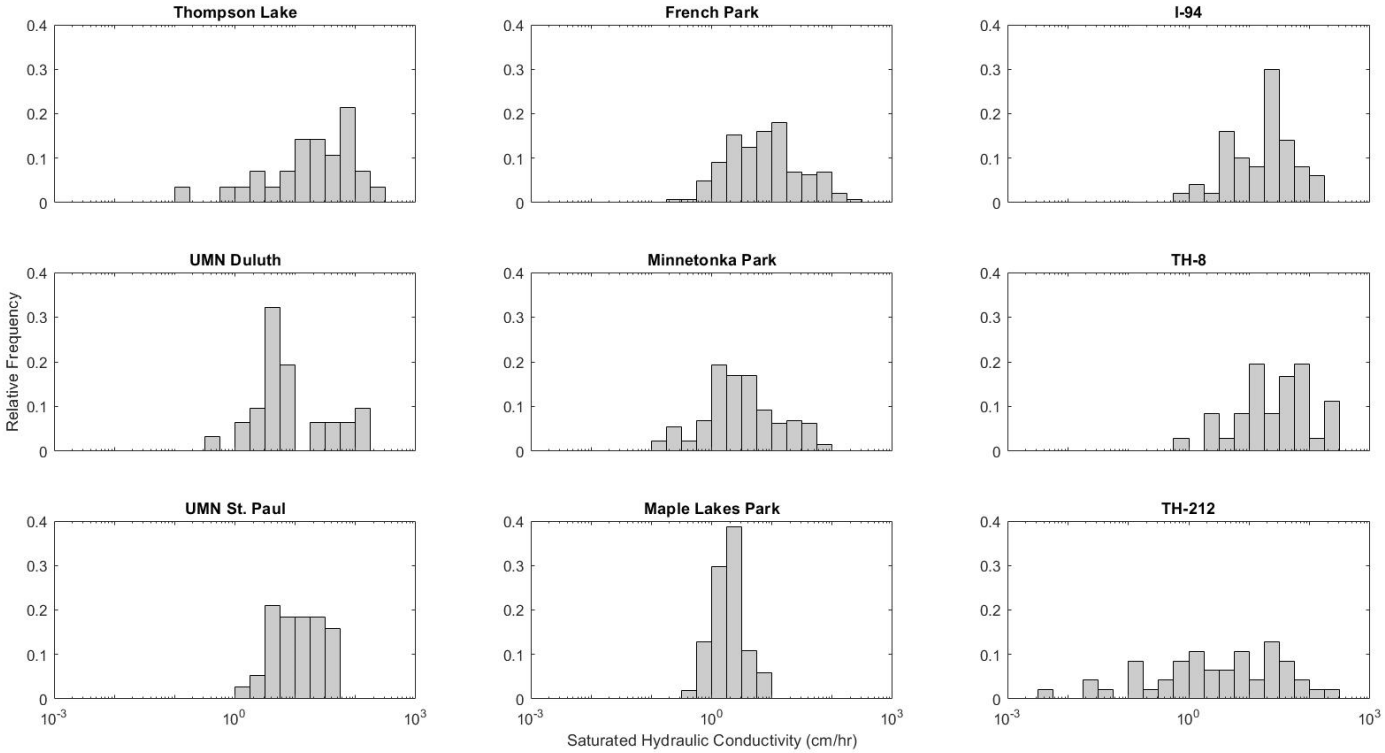

Figure 4.2 Relative frequency histograms of the K_{fs} at each site. All plots are displayed on a log-scale.

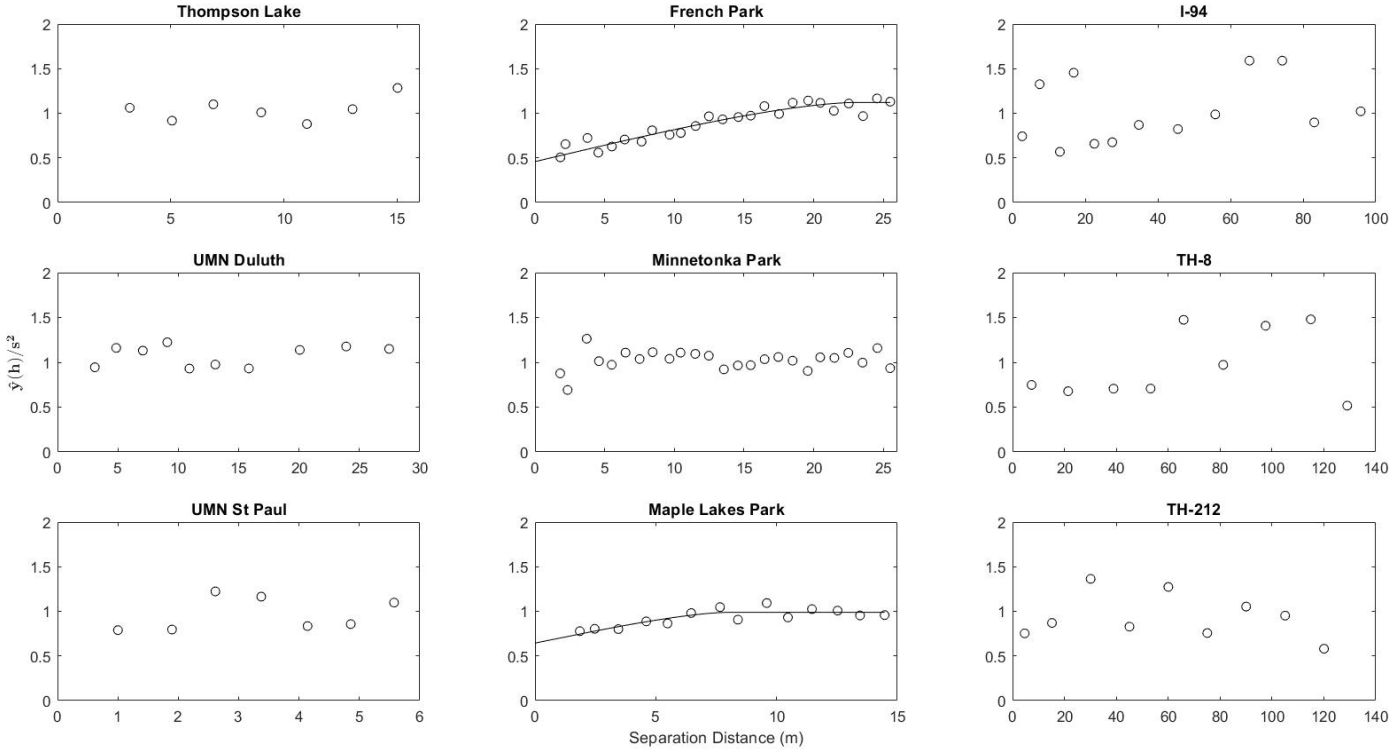

Figure 4.3 Variograms at each of the 9 sites. The variance at each separation distance h is normalized by the sample variance for the site. The solid lines show the theoretical variograms fit to the experimental data, when applicable. Plots that do not contain a solid line display a pure nugget effect.

Table 4.3 Theoretical variograms fit to the experimental variograms

	Minimum Separation Distance (m)	Pairs per Bin Minimum - Maximum	Theoretical Variogram Model	Nugget (-)	Sill (-)	Range (m)	r^2 (%)
Thompson Lake	3.2	29 - 44	Pure nugget	-	-	-	-
UMN Duluth	3.1	24-49	Pure nugget	-	-	-	-
UMN St. Paul	1.0	42 - 85	Pure nugget	-	-	-	-
French Park	1.8	53 - 482	Circular	0.45	1.12	22.7	90.2
Minnetonka Park	1.8	44 - 430	Pure nugget	-	-	-	-
Maple Lakes Park	1.9	50 - 375	Circular	0.64	0.99	7.9	71.7
I-94	2.7	34 - 88	Pure nugget	-	-	-	-
TH-8	7.4	34 - 59	Pure nugget	-	-	-	-
TH-212	4.7	41 – 71	Pure nugget	-	-	-	-

Several studies that estimated the surface or near surface horizontal spatial correlation range of K_{fs} in the literature are shown in Table 4.4, with a variety of land uses, scales, and methods. The most prevalent result for the spatial correlation range was either estimated to be between 7.9 meters and 35 meters or described by a pure nugget effect. Several of the studies discussed potential explanations of the K_{fs} variability. Variation in soil physical and chemical properties including bulk density, porosity, macropore density, organic matter content, particle size distribution, and exchangeable sodium percentage were cited as potential sources of variability in K_{fs} (Buttle & House, 1997; Duffera, White, & Weisz, 2007; Gwenzi, Hinz, Holmes, Phillips, & Mullins, 2011; Haws et al., 2004; Naitam, Kharche, Kadu, Mohrana, & Sharma, 2018; Sobieraj et al., 2002). The extent of several studies included multiple soil classifications, and the transition between soil classifications was suggested to contribute to the estimated range (Buttle & House, 1997; Haws et al., 2004). Studies also referred to natural, topographically influenced hydrologic processes such as erosion and deposition as contributing to the estimated range (Gupta et al., 2006; Haws et al., 2004; Iversen, Moldrup, Schjønning, & Jacobsen, 2003). Several of the studied land uses were managed systems, and the management practices (tillage, construction processes, etc.) were identified as potentially reducing the spatial correlation range (Duffera et al., 2007; Gwenzi et al., 2011; Haws et al., 2004; Naitam et al., 2018). The observed spatial correlation range in the present study, where most sites had a spatial correlation range of less than 5 meters, is towards the lower end relative to the other studies. This would seem reasonable as the GI in the present study was disturbed by excavation, import of fill, compaction, vehicle traffic, variable stormwater loading, vegetation lifecycles, and human activities resulting in a disconnection from the site's quaternary geology and thus a reduction in the spatial correlation range. Additional investigation of the causal relationship between natural processes, anthropogenic impacts, and spatial correlation range would be useful in developing effective methods to characterize K_{fs}.

Table 4.4 Comparison of surface or near surface horizontal spatial correlation range of K_{fs} between the present study and previous studies. Values separated by a hyphen represented the minimum and maximum reported values. The ampersand is used to separate discrete quantities.

Source	Land Use	n_{var}[a]	Method[b]	Support	Spacing[c]	Extent[d]	Range
Duffera et al., (2007)	Tobacco field	5	CHLP	45.4 cm^2	60 m	120,000 m^2	Pure nugget
Sobieraj et al., (2002)	Primary rainforest	4	AM	19.6 cm^2	25 m	525 m	Pure nugget
Haws et al., (2004)	Hay field	15	SRI & SSI	41.9 cm^2 – 10,000 cm^2	0.1 m – 10 m	1 m^2 90 m – 710 m	0.34 m – 209.4 m and pure nugget
Present Study	**Green Infrastructure**	**9**	**MPD**	**78.5 cm^2**	**1 m – 7.4 m**	**67 m^2 – 5,760 m^2**	**7.9 m & 22.7 m and pure nugget**
Gwenzi et al., (2011)	Bauxite residue disposal area	2	PD	78.5 cm^2	0.5 m	1,568 m^2	8 m and pure nugget
da Silva et al., (2017)	Fallow field	1	IP	Not reported	5 m	1,500 m^2	14.8 m
Gupta et al. (2006)	Plowed bare soil field	6	GP & DRI	33.2 cm^2 & 730.6 cm^2	8 m	5,824 m^2	9.8 m – 94.2 m
Buttle & House (1997)	Forested watershed	6	SRI & CHLP	314.2 cm^2 & 18.1 cm^2	15 m	32,200 m^2	15 m – 35 m and pure nugget
Loague & Gander (1990)	Native grassland pasture	7	SRI	7,853cm^2	2 m – 25 m	100,000 m^2 100 m – 250 m	<20 m and pure nugget
Iversen et al., (2003)	Winter wheat residue field	10	AP	314 cm^2	5 m	Not reported	30 m – >120 m and pure nugget
Awal et al., (2019)	No-till sweet corn field	1	TI	Not reported	10 m	20,800 m^2	32.5 m
Gao et al., (2012)	Scrubland & agricultural watershed	1	CHLP	19.6 cm^2	10 m	500,000 m^2	210 m
Naitam et al., (2018)	Agricultural Watershed	1	CHLP	Not reported	250 m	3,240,000 m^2	1183 m

a) n_{var} refers to the number of variograms from direct measures as reported in each study and may include multiple sites, soil horizons, or directional analyses. Variograms based on re-sampling are excluded.
b) Methods are abbreviated as follows: AM is Amoozemeter; AP is air permeameter; CHLP is constant head lab permeameter; DRI is double ring infiltrometer; GP is Guelph permeameter; IP is instantaneous profile; MPD is modified Philip-Dunne infiltrometer; PD is Philip-Dunne permeameter; SRI is single ring infiltrometer; SSI is single square infiltrometer; TI is tension infiltrometer
c) Spacing values are the minimum spacing reported for a given configuration
d) Extent values reported in linear units represent a 1-D transect, while square units represent a 2-D area

Application

Common engineering guidance for infiltration SCMs suggest that 1 infiltration point measurement should be completed for a given area to characterize K_{fs}. This guidance inherently assumes a level of homogeneity within the given area. The recommended frequency of measurements varies from 1 point per 19 m^2 (200 ft^2) (Center for Watershed Protection and Maryland Department of the Environment Water Management Administration, 2009), 1 point per 155 m^2 (1,667 ft^2) (Geosyntec Consultants & The City of San Diego, 2018), 1 point per 232 m^2 (2,500 ft^2) (Minnesota Pollution Control Agency, 2017), 1 point per 506 m^2 (5,445 ft^2) (Pennsylvania Department of Environmental Protection, 2006), 1 point per 929 m^2 (10,000 ft^2) (North Carolina Department of Environmental Quality, n.d.; Wisconsin Department of Natural Resources, 2017), to 1 point per 4645 m^2 (50,000 ft^2) (County of San Diego Department of Public Works, 2014). These areas, assuming a circular geometry, can be converted to an equivalent radius, which would be analogous to the spatial correlation range due to the assumed homogeneity. The equivalent radii are 2.4 m, 7.0 m, 8.6 m, 12.7 m, 17.2 m, and 38.5 m, respectively. Mulla & McBratney (2001) suggest that the smallest sample spacing should be ¼ to ½ the spatial correlation range to capture the spatial dependence. As seen in Table 4.3, the disturbed soils in this study have spatial correlation ranges that are typically less than equivalent radii typically provided as guidance for developing a sampling design.

In sampling designs where the spacing exceeds the spatial correlation range, the number of samples should be high enough that statistics that assume sampling independence can produce statistically significant results. The measured order of magnitude variability of K_{fs} as shown in Figure 4.2 and short correlation range shown in Figure 4.3 would suggest there would be a large uncertainty if a single measurement were extrapolated to represent a larger area. In an investigation of 4 swales, Ahmed, Gulliver, & Nieber (2015) found that 20 infiltration point measurements were required for the 95% confidence interval to be within a factor of 1.8 to 2.2 of the geometric mean, and that 40 infiltration point measurements were required for the 95% confidence interval to be within a factor of 1.5 to 1.7 of the geometric mean. As shown in Table 4.5, this study found that the multiplicative margin of error, equivalent to the 95% confidence interval normalized by the geometric mean, was within a factor of 1.1 to 2.0 for sample sizes ranging from 28 to 144. This agrees well with the findings of Ahmed et al. (2015) and supports

their observation that K_{fs} sampling designs based on a relatively limited number of samples will have a large associated uncertainty.

Table 4.5 The multiplicative margin of error of the geometric mean relative to the geometric mean

Site Name	Count	Multiplicative Margin of Error[a] at the 95% confidence level
Thompson Lake	28	1.9
UMN Duluth	31	1.6
UMN St. Paul	38	1.4
French Park	144	1.3
Minnetonka Park	130	1.3
Maple Lakes Park	101	1.1
I-94	50	1.4
TH-8	36	1.6
TH-212	47	2.0

a) The multiplicative margin of error is calculated as $\exp(z*\text{std}(\ln(x_i))/\text{sqrt}(n))$. This is equivalent to the 95% confidence interval normalized by the geometric mean.

Limitations

The following limitations should be noted:

1. Sampling at a sufficiently refined interval to capture the spatial structure at all sites would have been beneficial. However, the number of samples substantially exceed what is typically utilized to characterize infiltration SCM practices.
2. The results presented herein are only applicable to disturbed, urban systems. Natural or agricultural soils likely exhibit different spatial correlation structures.
3. Vertical variation of K_{fs} within the soil profile was not measured and vertical spatial correlation was not evaluated.

Conclusions

The spatial correlation range of K_{fs} in disturbed urban systems, typical of GI and infiltration SCMs, was estimated to vary from less than 1.0 meter to 22.7 meters, with 6 of the 9 sites having

a spatial correlation range less than 1 to 5 meters. Extrapolating the result of a single point measurement beyond the sampled soil volume has a large uncertainty. Systems that were constructed to be homogeneous such as rain gardens with an engineered media can show K_{fs} variability exceeding an order of magnitude over small separation distances. Variable disturbance, present in nearly all post construction systems, likely contributes to variable K_{fs}. Potential disturbances include excavation, import of fill, compaction, vehicle traffic, variable stormwater loading, vegetation lifecycles, and human activities.

Geostatistics are most appropriate when the sample spacing is ¼ to ½ the spatial correlation range. Therefore, a sample spacing of 0.25 to 1.25 meters may be necessary for many disturbed urban systems if geostatistics are used to characterize K_{fs}. Statistics that assume sampling independence may be most practical for characterizing K_{fs} in many disturbed systems, although large sample sizes may be required to reduce the uncertainty of the equivalent K_{fs} of a GI practice to an acceptable level. Even for small areas such as rain gardens, an adequate number of point measurements to allow for statistically significant results is important to characterize K_{fs}.

Chapter 5 Conclusions

Infiltration stormwater control measures (SCMs) have the potential to provide numerous hydrologic benefits to urban environments by promoting infiltration and evapotranspiration, processes that are not well represented in the water budget of urban areas. Infiltration SCMs mitigate the peak flow rate, reduce the runoff volume, and reduce the surface water pollutant loading relative to developed land uses without stormwater controls. The benefits of successful infiltration SCMs include flood mitigation, increased groundwater recharge, reduced erosion, increased green space, and promoting capture of dissolved and suspended pollutants. Unfortunately, infiltration SCMs presently have a relatively high failure rate which likely has slowed their rate of implementation. This research is focused on addressing several of the most common factors contributing to infiltration SCM failure.

A GIS based tool, referred to as the preliminary infiltration rating (PIR), was developed to identify potential locations that are likely able to support an infiltration SCM early in the planning or design phase. Chapter 2 describes how the PIR uses a fuzzy logic scheme to estimate the suitability of a site for a future infiltration SCM. The input datasets have broad coverage, allowing the PIR to be widely utilized throughout the United States. The output can be used as a planning tool that identifies regions of a development or municipality that are most likely able to support infiltration SCMs and to communicate those decisions between stakeholders. Additionally, the resolution is sufficiently refined that it can provide guidance to designers looking to site an infiltration SCM within a particular parcel. The PIR was estimated to predict an accurate or conservative estimate of the infiltration SCM performance in 85% of instances using a rain garden maintenance dataset to validate the tool. The PIR can be overlaid with other relevant project data including environmentally sensitive areas, property information, and proposed infrastructure to identify the areas that are most likely to be suitable for surface infiltration SCMs.

Chapter 3 and Chapter 4 both relate to estimating the in-situ infiltration capacity. The guidance in these chapters can be applied in the design phase, construction quality assurance, and as part of a monitoring and maintenance program. Chapter 3 estimates the systemic bias, i.e., the measured K_{sat} normalized by the true K_{sat}, for seven commonly used infiltration measurement methods. Numerical experiments are utilized as field measurements do not have an independent benchmark for which to compare the measured K_{sat}. The simulated methods had a bias that varied from 0.7 to

6.2 for soils ranging from sand through silt loam where infiltration SCMs tend to be located. Bias generally increased as soil texture shifted from coarse to fine. Methods that required smaller water volumes or shorter durations produced similar results to methods with larger water volumes or longer durations when the method accounted for laterally divergent flow paths. The cause of the systemic bias is suspected to be due to laterally divergent flows for methods that assume 1-dimensional flow, or differences between the assumed and true flow geometries for methods that assume 3-dimensional flow. Chapter 4 evaluates the horizontal spatial correlation range of K_{fs}, the distance at which measurements become spatially independent, at 9 sites typical of green infrastructure. A spatial correlation range of 7.9 and 22.7 meters were estimated for 2 of the sites. The other sites showed a pattern indicative of spatial independence indicating the spatial correlation likely occurred at a separation distance less than the sample spacing. Sample spacing at the sites varied from 1.0 meter to 7.4 meters. Therefore, the spatial correlation range typical of post-construction GI may vary from less than 1.0 meter to 22.7 meters, with 6 of the 9 sites having a spatial correlation range less than 5 meters. The spatial correlation range can be used to provide guidance on the development of sampling plans. When the systemic bias of infiltration measurement methods is considered in combination with the spatial correlation range, an extreme effort would be required for the margin of error on the estimated K_{fs} to be reduced to less than a factor of 2. Seasonal variations can also influence the infiltration rate on the order of a factor of 2 (Emerson & Traver, 2008). This should be considered in the design of infiltration SCMs through selecting an appropriate factor of safety on design infiltration rates and building conservatism into the design.

Infiltration SCMs have the potential to mitigate many of the adverse impacts of urbanization related to stormwater surface runoff. The goal of this research was to provide guidance that can assist in designing successful infiltration SCMs. Identifying potential infiltration areas early in the design phase allows the selected area to be integrated with other design elements. Characterizing the infiltration potential of an area requires an understanding of the accuracy of the selected method and understanding the spatial heterogeneity of a given site. This research is applicable throughout the land development process on project types including transportation, residential, commercial, industrial, and institutional development in both the public and private sectors.

References

Ahmed, F., Nestingen, R., Nieber, J. L., Gulliver, J. S., & Hozalski, R. M. (2014). A Modified Philip–Dunne Infiltrometer for Measuring the Field-Saturated Hydraulic Conductivity of Surface Soil. *Vadose Zone Journal*. https://doi.org/10.2136/vzj2014.01.0012

Ahmed, Farzana, Gulliver, J. S., & Nieber, J. L. (2015). Field Infiltration Measurements in Grassed Roadside Drainage Ditches: Spatial and Temporal Variability. *Journal of Hydrology*, *530*, 604–611. https://doi.org/10.1016/j.jhydrol.2015.10.012

Anoka Conservation District. (2019). Anoka Rain Gardens. Anoka Conservation District, Anoka, MN: Unpublished Data.

Asleson, B. C., Nestingen, R. S., Gulliver, J. S., Hozalski, R. M., & Nieber, J. L. (2009). Performance Assessment of Rain Gardens. *Journal of the American Water Resources Association*, *45*(4), 1019–1031.

ASTM International. (2018a). Standard Practice for Measuring Field Infiltration Rate and Calculating Field Hydraulic Conductivity Using the Modified Philip Dunne Infiltrometer Test. *ASTM International*, *D8152-18*, 1–13. https://doi.org/10.1520/D8152-18

ASTM International. (2018b). *Standard Test Method for Infiltration Rate of Soils in Field Using Double-Ring Infiltrometer*. *ASTM International* (Vol. D3385-18). https://doi.org/10.1520/D3385-18

Awal, R., Safeeq, M., Abbas, F., Fares, S., Deb, S. K., Ahmad, A., & Fares, A. (2019). Soil Physical Properties Spatial Variability under Long-Term No-Tillage Corn. *Agronomy*, *9*(11).

Bean, E. Z., & Dukes, M. D. (2016). Evaluation of Infiltration Basin Performance on Coarse Soils. *Journal of Hydrologic Engineering*, *21*(1), 1–9. https://doi.org/10.1061/(ASCE)HE.1943-5584.0001258

Blöschl, G., & Sivapalan, M. (1995). Scale issues in hydrological modelling: A review. *Hydrological Processes*, *9*(3–4), 251–290. https://doi.org/10.1002/hyp.3360090305

Booth, D. B. (1991). Urbanization and the Natural Drainage System--Impacts, Solutions, and

Prognoses. *The Northwest Environmental Journal*, *7*(93), 93–118.

Buttle, J. M., & House, D. A. (1997). Spatial variability of saturated hydraulic conductivity in shallow macroporous soils in a forested basin. *Journal of Hydrology*, *203*(1–4), 127–142. https://doi.org/10.1016/S0022-1694(97)00095-4

Cambardella, C. A., Moorman, T. B., Novak, J. M., Parkin, T. B., Karlen, D. L., Turco, R. F., & Konopka, A. E. (1994). Field-Scale Variability of Soil Properties in Central Iowa Soils. *Soil Science Society of America Journal*, *58*(5), 1501–1511. https://doi.org/10.2136/sssaj1994.03615995005800050033x

Carsel, R. F., & Parrish, R. S. (1988). Developing Joint Probability Distributions of Soil Water Retention Characteristics. *Water Resources Research*, *24*(5), 755–769.

Center for Watershed Protection and Maryland Department of the Environment Water Management Administration. (2009). *Maryland Stormwater Design Manual*. Baltimore, MD. Retrieved from https://mde.maryland.gov/programs/water/StormwaterManagementProgram/Pages/stormwater_design.aspx

COMSOL Multiphysics v. 5.4. (n.d.). Stockholm, Sweden: COMSOL AB. Retrieved from www.comsol.com

Congalton, R. G., Oderwald, R. G., & Mead, R. A. (1983). Assessing Landsat Classification Accuracy Using Discrete Multivariate Analysis Statistical Techniques. *Photogrammetric Engineering and Remote Sensing*, *49*(12), 1671–1678.

County of Los Angeles Department of Public Works. (2017). Guidelines for Geotechnical Investigation and Reporting Low Impact Development Stormwater Infiltration. Retrieved from https://dpw.lacounty.gov/gmed/permits/docs/policies/GS200.2.pdf

County of San Diego Department of Public Works. (2014). *Low Impact Development Handbook Stormwater Management Strategies*. Retrieved from https://www.sandiegocounty.gov/content/dam/sdc/dpw/WATERSHED_PROTECTION_PROGRAM/susmppdf/lid_handbook_2014sm.pdf

CTC & Associates LLC. (2018). *Infiltration Basins: Standards and Procedures to Ensure Performance*. Retrieved from http://dot.state.mn.us/research/TRS/2018/TRS1801.pdf

da Silva, A. C., Armindo, R. A., Brito, A. dos S., & Schaap, M. G. (2017). An Assessment of Pedotransfer Function Performance for the Estimation of Spatial Variability of Key Soil Hydraulic Properties. *Vadose Zone Journal*, *16*(9), vzj2016.12.0139. https://doi.org/10.2136/vzj2016.12.0139

Darcy, H. (1856). *Les fontaines publiques de la ville de Dijon: exposition et application...* Victor Dalmont.

Duffera, M., White, J. G., & Weisz, R. (2007). Spatial variability of Southeastern U.S. Coastal Plain soil physical properties: Implications for site-specific management. *Geoderma*, *137*, 327–339. https://doi.org/10.1016/j.geoderma.2006.08.018

Edaphic Scientific. (2021). SATURO dual head infiltrometer for saturated soil hydraulic conductivity. Retrieved August 1, 2021, from https://edaphic.com.au/products/soils/infiltrometer-dual-head/

Emerson, C. H., & Traver, R. G. (2008). Multiyear and Seasonal Variation of Infiltration from Storm-Water Best Management Practices. *Journal of Irrigation and Drainage Engineering*, *134*(5), 598–605. https://doi.org/10.1061/(ASCE)0733-9437(2008)134:5(598)

Gajem, Y. M., Warrick, A. W., & Myers, D. E. (1981). Spatial Dependence of Physical Properties of a Typic Torrifluvent Soil. *Soil Science Society of America Journal*, *45*(4), 709–715. https://doi.org/10.2136/sssaj1981.03615995004500040007x

Gao, L., Shao, M., & Wang, Y. (2012). Spatial scaling of saturated hydraulic conductivity of soils in a small watershed on the Loess Plateau, China. *Journal of Soils and Sediments*, *12*(6), 863–875. https://doi.org/10.1007/s11368-012-0511-3

García-Serrana, M., Gulliver, J. S., & Nieber, J. L. (2018). Calculator to Estimate Annual Infiltration Performance of Roadside Swales. *Journal of Hydrologic Engineering*, *23*(6), 04018017. https://doi.org/10.1061/(asce)he.1943-5584.0001650

Geosyntec Consultants, & The City of San Diego. (2018). *The City of San Diego Stormwater Standards*. Retrieved from https://www.sandiego.gov/sites/default/files/storm_water_standards_manual_oct_2018.pdf

Ghayoumian, J., Mohseni Saravi, M., Feiznia, S., Nouri, B., & Malekian, A. (2007). Application of GIS Techniques to Determine Areas Most Suitable for Artificial Groundwater Recharge

in a Coastal Aquifer in Southern Iran. *Journal of Asian Earth Sciences*, *30*(2), 364–374. https://doi.org/10.1016/j.jseaes.2006.11.002

Green, W. H., & Ampt, G. A. (1911). Studies on Soil Physics. Part 1 - The Flow of Air and Water Through Soils. *J. Agric. Sci*, *4*(1), 1–24.

Gupta, N., Rudra, R. P., & Parkin, G. (2006). Analysis of Spatial Variability of Hydraulic Conductivity at Field Scale. *Canadian Biosystems Engineering*, *48*(1), 55–62.

Gwenzi, W., Hinz, C., Holmes, K., Phillips, I. R., & Mullins, I. J. (2011). Field-scale spatial variability of saturated hydraulic conductivity on a recently constructed artificial ecosystem. *Geoderma*. https://doi.org/10.1016/j.geoderma.2011.06.010

Haws, N. W., Liu, B., Boast, C. W., Rao, P. S. C., Kladivko, E. J., & Franzmeier, D. P. (2004). Spatial Variability and Measurement Scale of Infiltration Rate on an Agricultural Landscape. *Soil Science Society of America Journal*, *68*(6), 1818–1826. https://doi.org/10.2136/sssaj2004.1818

Hilding, K. (1994). Longevity of Infiltration Basins Assessed in Puget Sound. *Watershed Protection Techniques*, *1*(3), 124–125.

Iversen, B. V, Moldrup, P., Schjønning, P., & Jacobsen, O. H. (2003). Field Application of a Portable Air Permeameter to Characterize Spatial Variability in Air and Water Permeability. *Vadose Zone Journal*.

Johnson, A. I. (1963). A Field Method for Measurement of Infiltration. *Geological Survey Water-Supply Paper*, *1544-F*, 27.

Kindred, J. S., & Reynolds, W. D. (2020). Using the borehole permeameter to estimate saturated hydraulic conductivity for glacially over-consolidated soils. *Hydrogeology Journal*.

Kirkwood, T. B. (1979). Geometric Means and Measures of Dispersion. *Biometrics*, *35*(4), 908–909.

Lai, J., & Ren, L. (2007). Assessing the Size Dependency of Measured Hydraulic Conductivity Using Double-Ring Infiltrometers and Numerical Simulation. *Soil Science Society of America Journal*, *71*(6), 1667–1675. https://doi.org/10.2136/sssaj2006.0227

Lee, R. S., Traver, R. G., & Welker, A. L. (2016). Evaluation of Soil Class Proxies for

Hydrologic Performance of In Situ Bioinfiltration Systems. *J. Sustainable Water Built Environ*, *2*(4), 1–10. https://doi.org/10.1061/JSWBAY.0000813

Lindsey, G., Roberts, L., & Page, W. (1992). Inspection and Maintenance of Infiltration Facilities. *Journal of Soil and Water Conservation*, *47*(6), 481–486.

Loague, K., & Gander, G. A. (1990). R-5 revisited: 1. Spatial variability of infiltration on a small rangeland catchment. *Water Resources Research*, *26*(5), 957–971. https://doi.org/10.1029/WR026i005p00957

MathWorks. (n.d.). lsqnonlin Solve nonlinear least-squares (nonlinear data-fitting) problems. Retrieved June 29, 2021, from https://www.mathworks.com/help/optim/ug/lsqnonlin.html

McBratney, A. B., & Webster, R. (1986). Choosing functions for semi-variograms of soil properties and fitting them to sampling estimates. *Journal of Soil Science*, *37*(4), 617–639. https://doi.org/10.1111/j.1365-2389.1986.tb00392.x

Meter Group. (2019). *Saturo*.

Miller, B. A. (2014). Semantic Calibration of Digital Terrain Analysis Scale. *Cartography and Geographic Information Science*, *41*(2), 166–176. https://doi.org/10.1080/15230406.2014.883488

Minnesota Department of Health. (2017). Drinking Water Supply Management Area Vulnerability. Retrieved from https://gisdata.mn.gov/dataset/water-drinking-water-supply

Minnesota Department of Health - Environmental Health Division - Source Water Protection Unit. (2014). Emergency Response Areas (ERA). Retrieved from https://gisdata.mn.gov/dataset/water-emergency-response-areas

Minnesota Department of Natural Resources. (n.d.). MnTOPO. Retrieved from https://www.dnr.state.mn.us/maps/mntopo/index.html

Minnesota Department of Natural Resources. (2016). Minnesota Regions Prone to Surface Karst Feature Development. Retrieved from https://gisdata.mn.gov/dataset/geos-surface-karst-feature-devel

Minnesota Department of Natural Resources. (2017). National Wetland Inventory Update for Minnesota. Retrieved from https://gisdata.mn.gov/dataset/water-nat-wetlands-inv-2009-

2014

Minnesota Department of Transportation. (2018). City Boundaries in Minnesota.

Minnesota Geologic Survey. (2016). Drift Thickness 2016. Retrieved from https://mngs-umn.opendata.arcgis.com/datasets/bb350c1d79d2416a966f5042213744ad

Minnesota Pollution Control Agency. (2017). *Minnesota Stormwater Manual*. Retrieved from https://stormwater.pca.state.mn.us/index.php/Main_Page

Minnesota Pollution Control Agency. (2018). *Construction Stormwater General Permit*. Retrieved from https://www.pca.state.mn.us/sites/default/files/wq-strm2-80a.pdf

Mulla, D. J., & McBratney, A. B. (2001). Soil Spatial Variability. In A. W. Warrick (Ed.), *Soil Physics Companions* (pp. 343–373). CRC Press.

Munoz-Carpena, R., Regalado, C. M. ., Alvares-Benedi, J., & Bartoli, F. (2002). Field Evaluation of the New Philip-Dunne Permeameter for Measuring Saturated Hydraulic Conductivity. *Soil Science*.

Naitam, R. K., Kharche, V. K., Kadu, P. R., Mohrana, P. C., & Sharma, R. P. (2018). Field-scale spatial variability of physical properties of black soils of Purna Valley, India, using Geostatistical Approach. *Journal of Soil and Water Conservation*, *17*(4), 325. https://doi.org/10.5958/2455-7145.2018.00050.4

Nimmo, J. R., Schmidt, K. M., Perkins, K. S., & Stock, J. D. (2009). Rapid Measurement of Field-Saturated Hydraulic Conductivity for Areal Characterization. *Vadose Zone Journal*. https://doi.org/10.2136/vzj2007.0159

North Carolina Department of Environmental Quality. (n.d.). *Stormwater Design Manual*. Retrieved from https://deq.nc.gov/about/divisions/energy-mineral-and-land-resources/stormwater/stormwater-program/stormwater-design

Olea, R. A. (2006). A six-step practical approach to semivariogram modeling. *Stochastic Environmental Research and Risk Assessment*, *20*, 307–318. https://doi.org/10.1007/s00477-005-0026-1

Olson, N. C., Gulliver, J. S., Nieber, J. L., & Kayhanian, M. (2013). Remediation to improve infiltration into compact soils. *Journal of Environmental Management*, *117*, 85–95.

Paus, K. H., Morgan, J., Gulliver, J. S., Leiknes, T., & Hozalski, R. M. (2014). Assessment of the Hydraulic and Toxic Metal Removal Capacities of Bioretention Cells after 2 to 8 Years of Service. *Water, Air, and Soil Pollution*, *225*(1), 1–12. https://doi.org/10.1007/s11270-013-1803-y

Pennsylvania Department of Environmental Protection. (2006). *Pennsylvania Stormwater Best Management Practices Manual*. Retrieved from http://www.depgreenport.state.pa.us/elibrary/GetFolder?FolderID=4673

Philip, J. R. (1992). Falling Head Ponded Infiltration. *Water Resources Research*, *28*(8), 2147–2148.

Philip, J. R. (1993). Approximate Analysis of Falling-Head Lined Borehole Permeameter. *Water Resources Research*. https://doi.org/10.1029/93WR01688

Pitt, R., Chen, S.-E., Clark, S., Swenson, J., & Ong, C. K. (2008). Compaction's Impacts on Urban Storm-Water Infiltration. *Journal of Irrigation and Drainage Engineering*, *134*(5), 652–658. https://doi.org/10.1061/(ASCE)0733-9437(2008)134

Press, J. (2019). *Determining the Minimum Number of Single-Ring Infiltration Tests Required to Reliably Predict Performance of a Rain Garden*. M.S. Thesis. Villanova University, Villanova, PA.

Rawls, W. J., Gimenez, D., & Grossman, R. (1998). Use of Soil Texture, Bulk Density, and Slope of the Water Retention Curve to Predict Saturated Hydraulic Conductivity. *American Society of Agricultural Engineers*, *41*(4), 983–988.

Reynolds, W. D. (2010). Measuring Soil Hydraulic Properties Using a Cased Borehole Permeameter: Steady Flow Analyses. *Vadose Zone Journal*, *9*, 637–652. https://doi.org/10.2136/vzj2009.0136

Reynolds, W. D., Bowman, B. T., Brunke, R. R., Drury, C. F., & Tan, C. S. (2000). Comparison of Tension Infiltrometer, Pressure Infiltrometer, and Soil Core Estimates of Saturated Hydraulic Conductivity. *Soil Science Society of America Journal*, *64*(2), 478–484. https://doi.org/10.2136/sssaj2000.642478x

Reynolds, W. D., & Elrick, D. E. (1986). A Method for Simultaneous In Situ Measurement in the Vadose Zone of Field-Saturated Hydraulic Conductivity, Sorptivity and the Conductivity-

Pressure Head Relationship. *Groundwater Monitoring & Remediation*, *6*(1), 84–95.

Reynolds, W. D., & Elrick, D. E. (1990). Ponded Infiltration From a Single Ring: I. Analysis of Steady Flow. *Soil Science Society of America Journal*, *54*, 1233–1241. https://doi.org/10.2136/sssaj1990.03615995005400050006x

Richards, L. A. (1931). Capillary conduction of liquids through porous mediums. *Physics*, *1*(5), 318–333. https://doi.org/10.1063/1.1745010

Robinson, A. R., & Rohwer, C. (1957). Measurement of Canal Seepage. *Transactions of the American Society of Civil Engineers*, *122*(1), 347–363. https://doi.org/10.1061/taceat.0007491

Ross, T. J. (2017). *Fuzzy Logic with Engineering Applications* (4th ed.). John Wiley & Sons.

Rousseeuw, P. J. (1990). Robust Estimation and Identifying Outliers. In *Handbook of Statistical Methods for Engineers and Scientists* (pp. 16.1-16.24). New York: McGraw-Hill.

Sasidharan, S., Bradford, S. A., Šimůnek, J., DeJong, B., & Kraemer, S. R. (2018). Evaluating drywells for stormwater management and enhanced aquifer recharge. *Advances in Water Resources*, *116*(November 2017), 167–177. https://doi.org/10.1016/j.advwatres.2018.04.003

Sauer, V. B., Thomas, W. O., Stricker, V. A., & Wilson, K. V. (1983). *Flood Characteristics of Urban Watersheds in the United States. US Geological Survey Water Supply Paper 2207*.

Schwanghart, W. (2021). variogramfit. Retrieved May 13, 2021, from https://www.mathworks.com/matlabcentral/fileexchange/25948-variogramfit

Sobieraj, J. A., Elsenbeer, H., Coelho, R. M., & Newton, B. (2002). Spatial variability of soil hydraulic conductivity along a tropical rainforest catena. *Geoderma*, *108*(1–2), 79–90. https://doi.org/10.1016/S0016-7061(02)00122-2

Soilmoisture Equipment Corp. (2012). *Guelph Permeameter – Operating Instructions*.

Turf-Tec International. (n.d.). *Turf-Tec Infiltrometer IN-2 Instructions*. Tallahassee, FL. Retrieved from http://www.turf-tec.com/Instructions/IN2-W Instructions_2017.pdf

U.S. Department of Agriculture, N. R. C. S. (2019). Soil Survey Geographic (SSURGO) database for Anoka, Dakota, Ramsey, and Washington Counties, Minnesota. U.S. Department of Agriculture, Natural Resources Conservation Service.

U.S. Environmental Protection Agency. (2020). What is Green Infrastructure? Retrieved July 12, 2021, from https://www.epa.gov/green-infrastructure/what-green-infrastructure

USBR 7300-89. (1989). *Procedure for Performing Field Permeability Testing by the Well Permeameter Method*.

van Genuchten, M. T. (1980). A Closed-form Equation for Predicting the Hydraulic Conductivity of Unsaturated Soils. *Soil Science Society of America Journal*, *44*(5), 892–898. https://doi.org/10.2136/sssaj1980.03615995004400050002x

Vogel, T., van Genuchten, M. T., & Cislerova, M. (2001). Effect of the shape of the soil hydraulic functions near saturation on variably-saturated flow predictions. *Advances in Water Resources*, *24*, 133–144.

Washington State Department of Ecology. (2019). *Stormwater Management Manual for Western Washington*. Retrieved from https://fortress.wa.gov/ecy/ezshare/wq/Permits/Flare/2019SWMMWW/2019SWMMWW.htm

Webster, R., & Oliver, A. M. (2007). *Geostatistics for Environmental Scientists*. (S. Senn, M. Scott, & V. Barnett, Eds.) (Second Edi). John Wiley & Sons.

Wisconsin Department of Natural Resources. (2017). *Conservation Practice Standard 1002 Site Evaluation for Stormwater Infiltration*. Retrieved from https://dnr.wi.gov/topic/stormwater/documents/1002SiteEvalForInfiltr.pdf

Zhang, Z. F., Groenevelt, P. H., & Parkin, G. W. (1998). The well-shape factor for the measurement of soil hydraulic properties using the Guelph Permeameter. *Soil and Tillage Research*, *49*(3), 219–221. https://doi.org/10.1016/S0167-1987(98)00174-3

Appendix A

Appendix A contains supporting information for Chapter 3

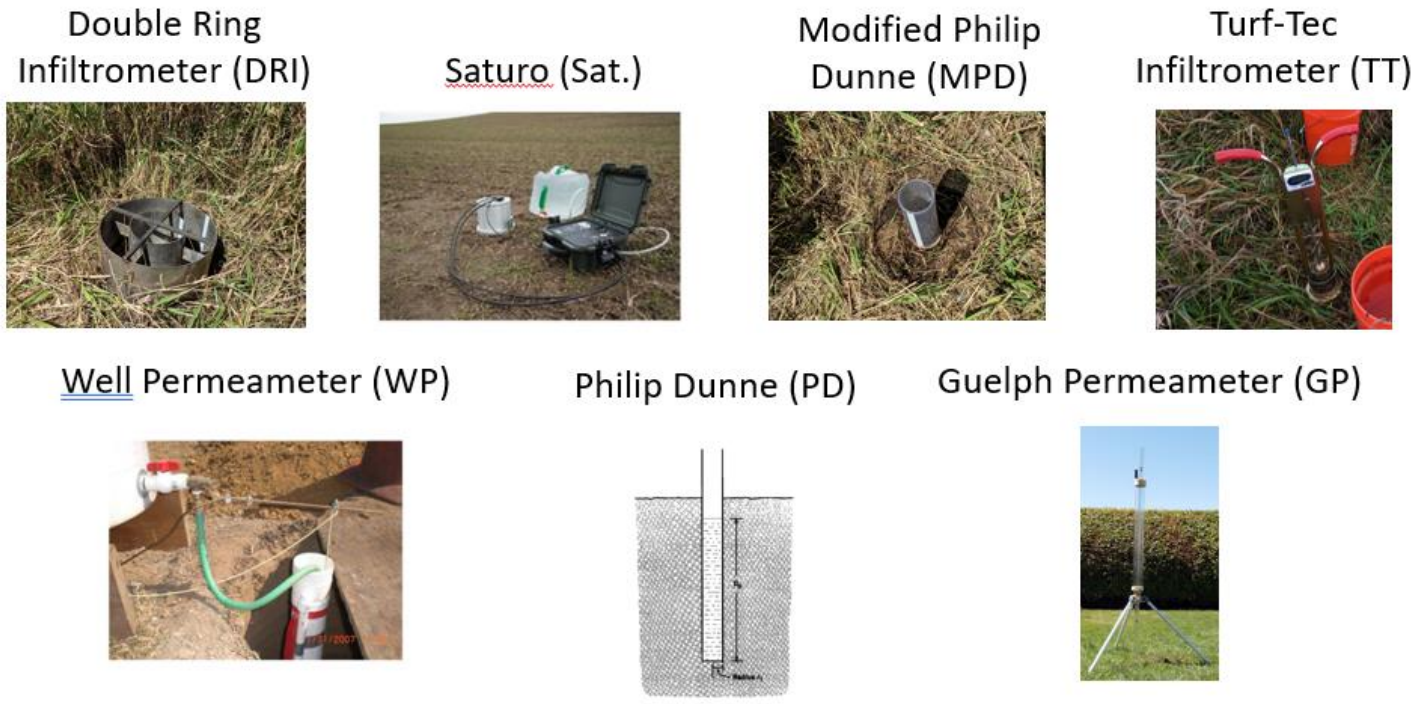

Figure A.1 The infiltration measurement methods that estimate K_{sat} in the numerical simulations. Images from (County of Los Angeles Department of Public Works, 2017; Edaphic Scientific, 2021; Philip, 1993; Soilmoisture Equipment Corp., 2012)

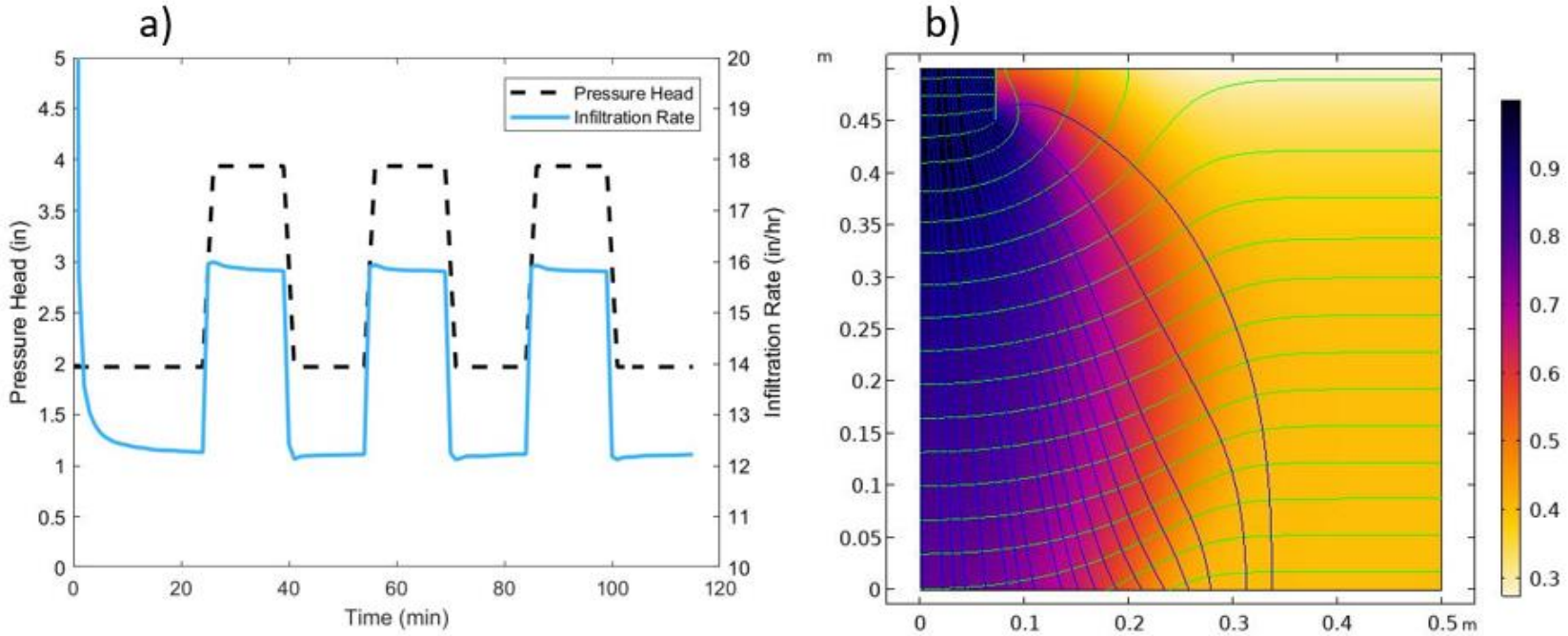

Figure A.2 Sample output from the numerical experiments in COMSOL. The experiment displayed is the Saturo infiltrometer with loamy sand soil at an initial relative soil moisture of 41%. a) the time variable pressure head boundary condition applied within the single ring to implement the dual head procedure and the time variable infiltration rate. b) the volumetric water content within the simulated soil domain at the end of the numerical experiment is displayed in the color ramp, while the lines represent a flow net.

Table A.1 Double Ring Infiltrometer (DRI) Duration of Test and Bias. K_{sat} is the saturated hydraulic conductivity, H_{p0} is the initial soil water pressure head, S_{e0} is the initial relative soil moisture, Bias is the "measured" K_{sat} divided by the input K_{sat}.

Soil Texture	K_{sat} (m/s)	H_{p0} (m)	S_{e0} (m^3/m^3)	Duration of Test (hrs)	Bias
Sand	8.25E-05	-0.05	0.8199	6.00	1.18
Sand	8.25E-05	-0.0752	0.6132	6.00	1.18
Sand	8.25E-05	-0.1079	0.4087	6.00	1.18
Sand	8.25E-05	-0.1745	0.2045	6.00	1.18
Loamy Sand	4.05E-05	-0.0589	0.8184	6.00	1.18
Loamy Sand	4.05E-05	-0.0958	0.6143	6.00	1.18
Loamy Sand	4.05E-05	-0.1499	0.4095	6.00	1.18
Loamy Sand	4.05E-05	-0.2762	0.2048	6.00	1.18
Sandy Loam	1.23E-05	-0.1023	0.8104	6.00	1.20
Sandy Loam	1.23E-05	-0.1901	0.6081	6.00	1.20
Sandy Loam	1.23E-05	-0.3438	0.4054	6.00	1.20
Sandy Loam	1.23E-05	-0.7985	0.2027	6.00	1.20
Sandy Clay Loam	3.64E-06	-0.1682	0.8110	6.00	1.19
Sandy Clay Loam	3.64E-06	-0.42	0.6081	6.00	1.20
Sandy Clay Loam	3.64E-06	-1.0966	0.4055	6.00	1.20
Sandy Clay Loam	3.64E-06	-4.7953	0.2033	6.00	1.21
Silt Loam	1.25E-06	-0.5526	0.8028	6.00	1.29
Silt Loam	1.25E-06	-1.5184	0.6020	6.00	1.37
Silt Loam	1.25E-06	-4.5058	0.4021	6.00	1.48
Silt Loam	1.25E-06	-10	0.2925	6.58	1.53
Sandy Clay	3.33E-07	-0.7278	0.8042	6.00	1.36
Sandy Clay	3.33E-07	-3.2146	0.6037	7.25	1.59
Sandy Clay	3.33E-07	-7.5	0.5009	8.25	1.69
Sandy Clay	3.33E-07	-10	0.4695	8.17	1.76
Silty Clay	5.56E-08	-2.5	0.9349	9.83	2.13
Silty Clay	5.56E-08	-5	0.8978	10.92	2.65
Silty Clay	5.56E-08	-7.5	0.8729	11.17	3.06
Silty Clay	5.56E-08	-10	0.8543	11.50	3.37

Table A.2 Saturo (SAT) Infiltrometer Duration of Test and Bias. K_{sat} is the saturated hydraulic conductivity, H_{p0} is the initial soil water pressure head, S_{e0} is the initial relative soil moisture, Bias is the "measured" K_{sat} divided by the input K_{sat}.

Soil Texture	K_{sat} (m/s)	H_{p0} (m)	S_{e0} (m^3/m^3)	Duration of Test (hrs)	Bias
Sand	8.25E-05	-0.05	0.8199	1.92	1.16
Sand	8.25E-05	-0.0752	0.6132	1.92	1.16
Sand	8.25E-05	-0.1079	0.4087	1.92	1.16
Sand	8.25E-05	-0.1745	0.2045	1.92	1.16
Loamy Sand	4.05E-05	-0.0589	0.8184	1.92	1.17
Loamy Sand	4.05E-05	-0.0958	0.6143	1.92	1.17
Loamy Sand	4.05E-05	-0.1499	0.4095	1.92	1.17
Loamy Sand	4.05E-05	-0.2762	0.2048	1.92	1.17
Sandy Loam	1.23E-05	-0.1023	0.8104	1.92	1.18
Sandy Loam	1.23E-05	-0.1901	0.6081	1.92	1.20
Sandy Loam	1.23E-05	-0.3438	0.4054	1.92	1.21
Sandy Loam	1.23E-05	-0.7985	0.2027	1.92	1.22
Sandy Clay Loam	3.64E-06	-0.1682	0.8110	1.92	1.22
Sandy Clay Loam	3.64E-06	-0.42	0.6081	1.92	1.25
Sandy Clay Loam	3.64E-06	-1.0966	0.4055	1.92	1.28
Sandy Clay Loam	3.64E-06	-4.7953	0.2033	1.92	1.30
Silt Loam	1.25E-06	-0.5526	0.8028	2.50	1.29
Silt Loam	1.25E-06	-1.5184	0.6020	2.50	1.34
Silt Loam	1.25E-06	-4.5058	0.4021	2.50	1.38
Silt Loam	1.25E-06	-10	0.2925	2.50	1.39
Sandy Clay	3.33E-07	-0.7278	0.8042	3.00	1.32
Sandy Clay	3.33E-07	-3.2146	0.6037	3.00	1.45
Sandy Clay	3.33E-07	-7.5	0.5009	3.00	1.45
Sandy Clay	3.33E-07	-10	0.4695	3.00	1.49
Silty Clay	5.56E-08	-2.5	0.9349	3.00	1.68
Silty Clay	5.56E-08	-5	0.8978	3.00	1.84
Silty Clay	5.56E-08	-7.5	0.8729	3.00	2.03
Silty Clay	5.56E-08	-10	0.8543	3.00	2.27

Table A.3 Modified Philip Dunne (MPD) Infiltrometer Duration of Test and Bias. K_{sat} is the saturated hydraulic conductivity, H_{p0} is the initial soil water pressure head, S_{e0} is the initial relative soil moisture, Bias is the "measured" K_{sat} divided by the input K_{sat}.

Soil Texture	K_{sat} (m/s)	H_{p0} (m)	S_{e0} (m^3/m^3)	Duration of Test (hrs)	Bias
Sand	8.25E-05	-0.05	0.8199	0.32	1.02
Sand	8.25E-05	-0.0752	0.6132	0.32	1.04
Sand	8.25E-05	-0.1079	0.4087	0.32	0.98
Sand	8.25E-05	-0.1745	0.2045	0.32	1.02
Loamy Sand	4.05E-05	-0.0589	0.8184	0.63	0.99
Loamy Sand	4.05E-05	-0.0958	0.6143	0.63	0.97
Loamy Sand	4.05E-05	-0.1499	0.4095	0.63	1.01
Loamy Sand	4.05E-05	-0.2762	0.2048	0.63	1.00
Sandy Loam	1.23E-05	-0.1023	0.8104	2.05	0.98
Sandy Loam	1.23E-05	-0.1901	0.6081	2.00	0.95
Sandy Loam	1.23E-05	-0.3438	0.4054	1.98	0.97
Sandy Loam	1.23E-05	-0.7985	0.2027	1.97	0.99
Sandy Clay Loam	3.64E-06	-0.1682	0.8110	6.92	0.99
Sandy Clay Loam	3.64E-06	-0.42	0.6081	6.68	0.96
Sandy Clay Loam	3.64E-06	-1.0966	0.4055	6.68	1.01
Sandy Clay Loam	3.64E-06	-4.7953	0.2033	6.13	1.05
Silt Loam	1.25E-06	-0.5526	0.8028	15.82	0.95
Silt Loam	1.25E-06	-1.5184	0.6020	15.23	1.01
Silt Loam	1.25E-06	-4.5058	0.4021	14.70	1.02
Silt Loam	1.25E-06	-10	0.2925	13.50	1.08
Sandy Clay	3.33E-07	-0.7278	0.8042	24.00	0.88
Sandy Clay	3.33E-07	-3.2146	0.6037	24.00	0.88
Sandy Clay	3.33E-07	-7.5	0.5009	24.00	1.08
Sandy Clay	3.33E-07	-10	0.4695	24.00	1.73
Silty Clay	5.56E-08	-2.5	0.9349	24.00	1.71
Silty Clay	5.56E-08	-5	0.8978	24.00	1.86
Silty Clay	5.56E-08	-7.5	0.8729	24.00	1.92
Silty Clay	5.56E-08	-10	0.8543	24.00	1.96

Table A.4 Turf-Tec (TT) Infiltrometer Duration of Test and Bias. K_{sat} is the saturated hydraulic conductivity, H_{p0} is the initial soil water pressure head, S_{e0} is the initial relative soil moisture, Bias is the "measured" K_{sat} divided by the input K_{sat}.

Soil Texture	K_{sat} (m/s)	H_{p0} (m)	S_{e0} (m^3/m^3)	Duration of Test (hrs)	Bias
Sand	8.25E-05	-0.05	0.8199	0.44	2.15
Sand	8.25E-05	-0.0752	0.6132	0.44	2.15
Sand	8.25E-05	-0.1079	0.4087	0.44	2.16
Sand	8.25E-05	-0.1745	0.2045	0.44	2.16
Loamy Sand	4.05E-05	-0.0589	0.8184	0.50	2.44
Loamy Sand	4.05E-05	-0.0958	0.6143	0.50	2.44
Loamy Sand	4.05E-05	-0.1499	0.4095	0.50	2.45
Loamy Sand	4.05E-05	-0.2762	0.2048	0.50	2.46
Sandy Loam	1.23E-05	-0.1023	0.8104	0.50	2.92
Sandy Loam	1.23E-05	-0.1901	0.6081	0.50	2.98
Sandy Loam	1.23E-05	-0.3438	0.4054	0.50	3.02
Sandy Loam	1.23E-05	-0.7985	0.2027	0.50	3.05
Sandy Clay Loam	3.64E-06	-0.1682	0.8110	0.50	3.13
Sandy Clay Loam	3.64E-06	-0.42	0.6081	0.50	3.27
Sandy Clay Loam	3.64E-06	-1.0966	0.4055	0.50	3.37
Sandy Clay Loam	3.64E-06	-4.7953	0.2033	0.50	3.65
Silt Loam	1.25E-06	-0.5526	0.8028	0.50	4.08
Silt Loam	1.25E-06	-1.5184	0.6020	0.50	4.65
Silt Loam	1.25E-06	-4.5058	0.4021	0.50	5.34
Silt Loam	1.25E-06	-10	0.2925	0.50	6.21
Sandy Clay	3.33E-07	-0.7278	0.8042	0.50	4.72
Sandy Clay	3.33E-07	-3.2146	0.6037	0.50	6.70
Sandy Clay	3.33E-07	-7.5	0.5009	0.50	8.15
Sandy Clay	3.33E-07	-10	0.4695	0.50	9.10
Silty Clay	5.56E-08	-2.5	0.9349	0.50	11.07
Silty Clay	5.56E-08	-5	0.8978	0.50	15.14
Silty Clay	5.56E-08	-7.5	0.8729	0.50	18.01
Silty Clay	5.56E-08	-10	0.8543	0.50	20.28

Table A.5 USBR Well Permeameter (WP) Duration of Test and Bias. K_{sat} is the saturated hydraulic conductivity, H_{p0} is the initial soil water pressure head, S_{e0} is the initial relative soil moisture, Bias is the "measured" K_{sat} divided by the input K_{sat}.

Soil Texture	K_{sat} (m/s)	H_{p0} (m)	S_{e0} (m^3/m^3)	Duration of Test (hrs)	Bias
Sand	8.25E-05	-0.05	0.8199	6.00	1.37
Sand	8.25E-05	-0.0752	0.6132	6.00	1.37
Sand	8.25E-05	-0.1079	0.4087	6.00	1.37
Sand	8.25E-05	-0.1745	0.2045	6.00	1.37
Loamy Sand	4.05E-05	-0.0589	0.8184	6.00	1.39
Loamy Sand	4.05E-05	-0.0958	0.6143	6.00	1.39
Loamy Sand	4.05E-05	-0.1499	0.4095	6.00	1.39
Loamy Sand	4.05E-05	-0.2762	0.2048	6.00	1.39
Sandy Loam	1.23E-05	-0.1023	0.8104	6.00	1.45
Sandy Loam	1.23E-05	-0.1901	0.6081	6.00	1.47
Sandy Loam	1.23E-05	-0.3438	0.4054	6.00	1.49
Sandy Loam	1.23E-05	-0.7985	0.2027	6.00	1.50
Sandy Clay Loam	3.64E-06	-0.1682	0.8110	6.00	1.46
Sandy Clay Loam	3.64E-06	-0.42	0.6081	6.00	1.52
Sandy Clay Loam	3.64E-06	-1.0966	0.4055	6.00	1.57
Sandy Clay Loam	3.64E-06	-4.7953	0.2033	6.00	1.60
Silt Loam	1.25E-06	-0.5526	0.8028	9.58	1.89
Silt Loam	1.25E-06	-1.5184	0.6020	8.08	2.13
Silt Loam	1.25E-06	-4.5058	0.4021	7.08	2.30
Silt Loam	1.25E-06	-10	0.2925	6.00	2.42
Sandy Clay	3.33E-07	-0.7278	0.8042	24.00	1.73
Sandy Clay	3.33E-07	-3.2146	0.6037	24.00	1.90
Sandy Clay	3.33E-07	-7.5	0.5009	24.00	1.98
Sandy Clay	3.33E-07	-10	0.4695	19.42	2.05
Silty Clay	5.56E-08	-2.5	0.9349	24.00	3.09
Silty Clay	5.56E-08	-5	0.8978	24.00	3.55
Silty Clay	5.56E-08	-7.5	0.8729	24.00	3.81
Silty Clay	5.56E-08	-10	0.8543	24.00	4.00

Table A.6 Philip Dunne (PD) Permeameter Duration of Test and Bias. K_{sat} is the saturated hydraulic conductivity, H_{p0} is the initial soil water pressure head, S_{e0} is the initial relative soil moisture, Bias is the "measured" K_{sat} divided by the input K_{sat}.

Soil Texture	K_{sat} (m/s)	H_{p0} (m)	S_{e0} (m^3/m^3)	Duration of Test (hrs)	Bias
Sand	8.25E-05	-0.05	0.8199	0.17	0.75
Sand	8.25E-05	-0.0752	0.6132	0.15	0.73
Sand	8.25E-05	-0.1079	0.4087	0.15	0.74
Sand	8.25E-05	-0.1745	0.2045	0.15	0.74
Loamy Sand	4.05E-05	-0.0589	0.8184	0.33	0.75
Loamy Sand	4.05E-05	-0.0958	0.6143	0.32	0.75
Loamy Sand	4.05E-05	-0.1499	0.4095	0.32	0.76
Loamy Sand	4.05E-05	-0.2762	0.2048	0.30	0.77
Sandy Loam	1.23E-05	-0.1023	0.8104	1.03	0.78
Sandy Loam	1.23E-05	-0.1901	0.6081	0.97	0.78
Sandy Loam	1.23E-05	-0.3438	0.4054	0.95	0.80
Sandy Loam	1.23E-05	-0.7985	0.2027	0.92	0.80
Sandy Clay Loam	3.64E-06	-0.1682	0.8110	3.40	0.80
Sandy Clay Loam	3.64E-06	-0.42	0.6081	3.23	0.82
Sandy Clay Loam	3.64E-06	-1.0966	0.4055	3.12	0.83
Sandy Clay Loam	3.64E-06	-4.7953	0.2033	2.80	1.06
Silt Loam	1.25E-06	-0.5526	0.8028	7.47	0.86
Silt Loam	1.25E-06	-1.5184	0.6020	6.78	0.86
Silt Loam	1.25E-06	-4.5058	0.4021	6.27	0.83
Silt Loam	1.25E-06	-10	0.2925	5.73	1.14
Sandy Clay	3.33E-07	-0.7278	0.8042	24.00	0.80
Sandy Clay	3.33E-07	-3.2146	0.6037	24.00	0.85
Sandy Clay	3.33E-07	-7.5	0.5009	24.00	1.05
Sandy Clay	3.33E-07	-10	0.4695	24.00	1.42
Silty Clay	5.56E-08	-2.5	0.9349	24.00	1.08
Silty Clay	5.56E-08	-5	0.8978	24.00	1.21
Silty Clay	5.56E-08	-7.5	0.8729	24.00	1.32
Silty Clay	5.56E-08	-10	0.8543	24.00	1.58

Table A.7 Guelph Permeameter (GP) Duration of Test and Bias. K_{sat} is the saturated hydraulic conductivity, H_{p0} is the initial soil water pressure head, S_{e0} is the initial relative soil moisture, Bias is the "measured" K_{sat} divided by the input K_{sat}.

Soil Texture	K_{sat} (m/s)	H_{p0} (m)	S_{e0} (m^3/m^3)	Duration of Test (hrs)	Bias
Sand	8.25E-05	-0.05	0.8199	0.50	1.05
Sand	8.25E-05	-0.0752	0.6132	0.78	1.05
Sand	8.25E-05	-0.1079	0.4087	0.98	1.06
Sand	8.25E-05	-0.1745	0.2045	1.15	1.06
Loamy Sand	4.05E-05	-0.0589	0.8184	0.70	1.05
Loamy Sand	4.05E-05	-0.0958	0.6143	1.08	1.06
Loamy Sand	4.05E-05	-0.1499	0.4095	1.35	1.07
Loamy Sand	4.05E-05	-0.2762	0.2048	1.57	1.08
Sandy Loam	1.23E-05	-0.1023	0.8104	1.38	1.08
Sandy Loam	1.23E-05	-0.1901	0.6081	2.15	1.10
Sandy Loam	1.23E-05	-0.3438	0.4054	2.62	1.13
Sandy Loam	1.23E-05	-0.7985	0.2027	2.98	1.14
Sandy Clay Loam	3.64E-06	-0.1682	0.8110	2.48	0.95
Sandy Clay Loam	3.64E-06	-0.42	0.6081	3.48	0.99
Sandy Clay Loam	3.64E-06	-1.0966	0.4055	4.07	1.02
Sandy Clay Loam	3.64E-06	-4.7953	0.2033	2.87	1.38
Silt Loam	1.25E-06	-0.5526	0.8028	4.60	1.07
Silt Loam	1.25E-06	-1.5184	0.6020	5.47	1.19
Silt Loam	1.25E-06	-4.5058	0.4021	6.07	1.23
Silt Loam	1.25E-06	-10	0.2925	6.32	1.30
Sandy Clay	3.33E-07	-0.7278	0.8042	6.25	1.15
Sandy Clay	3.33E-07	-3.2146	0.6037	7.32	1.31
Sandy Clay	3.33E-07	-7.5	0.5009	8.32	1.35
Sandy Clay	3.33E-07	-10	0.4695	7.87	1.41
Silty Clay	5.56E-08	-2.5	0.9349	7.78	1.65
Silty Clay	5.56E-08	-5	0.8978	8.85	1.88
Silty Clay	5.56E-08	-7.5	0.8729	9.08	2.20
Silty Clay	5.56E-08	-10	0.8543	9.85	2.14

Appendix B

Supporting information for Chapter 4

Table B.1 Descriptive statistics for evaluated sites, using the full dataset inclusive of outliers

	Count (-)	Arithmetic Mean (cm/hr)	Standard Deviation (cm/hr)	Geometric Mean (cm/hr)	Geometric Standard Deviation (-)	Minimum (cm/hr)	Maximum (cm/hr)
Thompson Lake	29	45.0	53.7	13.3	11.1	0.0025	194.6
UMN Duluth	34	32.6	58.0	7.6	8.2	0.0025	229.1
UMN St. Paul	39	15.6	13.8	8.8	5.1	0.0025	54.5
French Park	145	18.3	31.1	7.1	4.2	0.06	218.2
Minnetonka Park	132	9.9	19.1	3.3	4.4	0.12	120.5
Maple Lakes Park	102	2.3	1.6	1.8	1.9	0.21	9.2
I-94	51	27.5	27.9	15.0	3.6	0.27	114.0
TH-8	37	55.5	73.1	22.2	5.3	0.08	271.7
TH-212	47	18.5	37.1	2.8	11.9	0.004	204.4

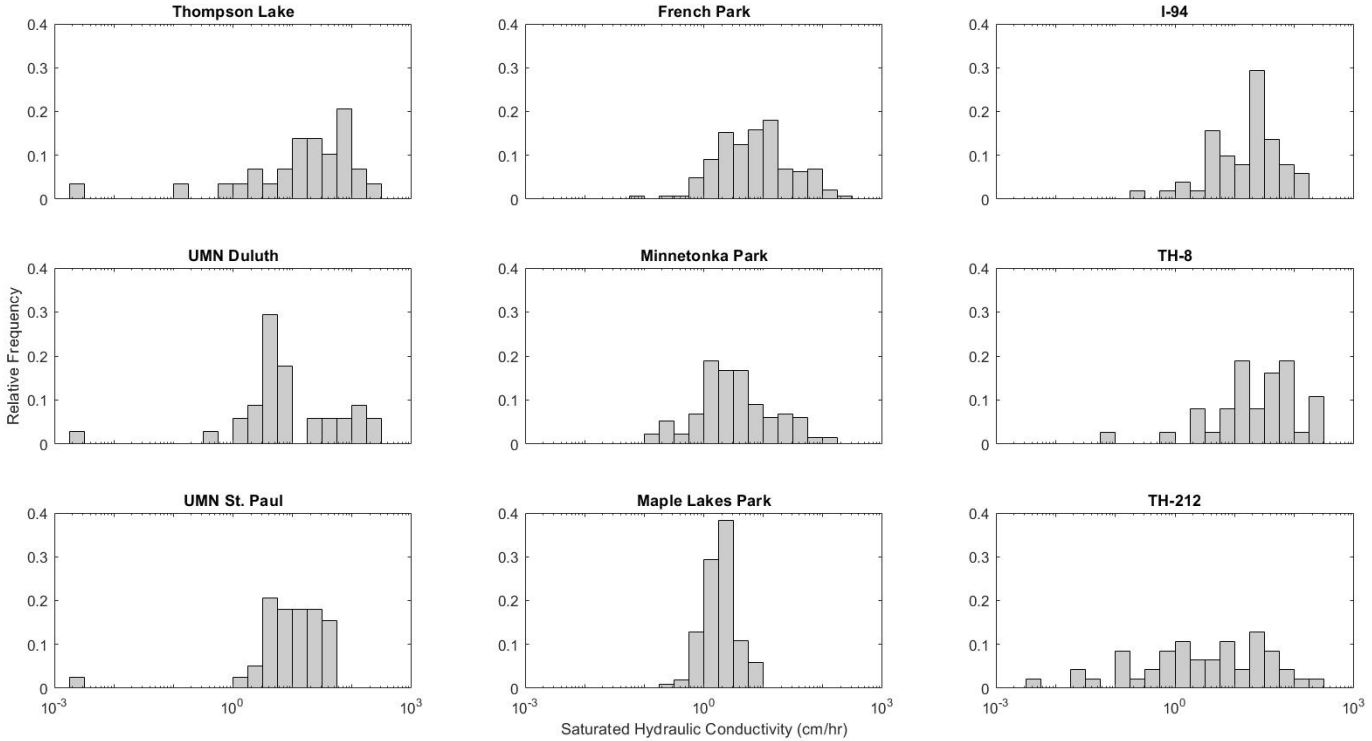

Figure B.1 Relative frequency histograms of the K_{fs} at each site. All plots are displayed on a log-scale, using the full dataset inclusive of outliers.

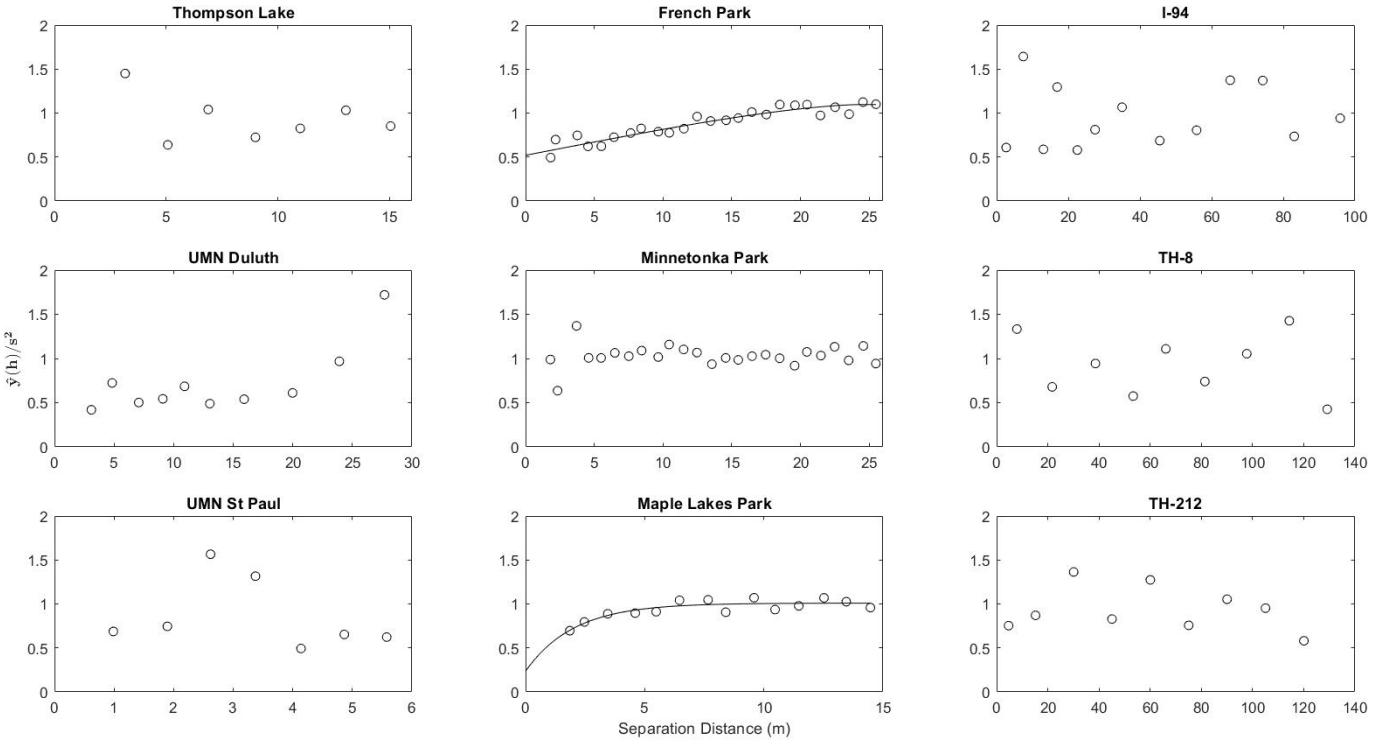

Figure B.2 Variograms at each of the 9 sites. The variance at each separation distance h is normalized by the sample variance for the site. The solid lines show the theoretical variograms fit to the experimental data, when applicable. Plots that do not contain a solid line display a pure nugget effect. Variograms are constructed using the full dataset inclusive of outliers.

Table B.2 Theoretical variograms fit to the experimental variograms, using the full dataset inclusive of outliers.

	Minimum Separation Distance (m)	Pairs per Bin Minimum - Maximum	Theoretical Variogram Model	Nugget (-)	Sill (-)	Range (m)	r^2 (%)
Thompson Lake	3.2	30 – 48	Pure nugget	-	-	-	-
UMN Duluth	3.1	29 – 53	Pure nugget	-	-	-	-
UMN St. Paul	1.0	43 – 91	Pure nugget	-	-	-	-
French Park	1.8	54 – 488	Circular	0.52	1.10	24.2	88.8
Minnetonka Park	1.8	48 – 447	Pure nugget	-	-	-	-
Maple Lakes Park	1.9	50 – 381	Exponential	0.24	1.01	6.1	76.2
I-94	2.7	35 – 94	Pure nugget	-	-	-	-
TH-8	7.9	35 – 66	Pure nugget	-	-	-	-
TH-212	4.7	41 – 71	Pure nugget	-	-	-	-

Table B.3 The multiplicative margin of error relative to the geometric mean, using the full dataset inclusive of outliers.

Site Name	Count	Multiplicative Margin of Error[a] at the 95% confidence level
Thompson Lake	29	2.4
UMN Duluth	34	2.0
UMN St. Paul	39	1.7
French Park	145	1.3
Minnetonka Park	132	1.3
Maple Lakes Park	102	1.1
I-94	51	1.4
TH-8	37	1.7
TH-212	47	2.0

a) The multiplicative margin of error is calculated as $\exp(z*\text{std}(\ln(x_i))/\text{sqrt}(n))$. This is equivalent to the 95% confidence interval normalized by the geometric mean.